J. Fluid Mech. (1997), *vol.* 336, *pp.* 379–409

Mass transfer dominated by thermal diffusion in laminar boundary layers

By PEDRO L. GARCÍA-YBARRA AND JOSE L. CASTILLO

Departamento Física, LCDI, Universidad Nacional de Educación a Distancia, Apdo 60141, Madrid 28080, Spain

(Received 30 May 1995 and in revised form 14 October 1996)

The concentration distribution of massive dilute species (e.g. aerosols, heavy vapours, etc.) carried in a gas stream in non-isothermal boundary layers is studied in the large-Schmidt-number limit, $Sc \gg 1$, including the cross-mass-transport by thermal diffusion (Ludwig–Soret effect). In self-similar laminar boundary layers, the mass fraction distribution of the dilute species is governed by a second-order ordinary differential equation whose solution becomes a singular perturbation problem when $Sc \gg 1$. Depending on the sign of the temperature gradient, the solutions exhibit different qualitative behaviour. First, when the thermal diffusion transport is directed toward the wall, the boundary layer can be divided into two separated regions: an outer region characterized by the cooperation of advection and thermal diffusion and an inner region in the vicinity of the wall, where Brownian diffusion accommodates the mass fraction to the value required by the boundary condition at the wall. Secondly, when the thermal diffusion transport is directed away from the wall, thus competing with the advective transport, both effects balance each other at some intermediate value of the similarity variable and a thin intermediate diffusive layer separating two outer regions should be considered around this location. The character of the outer solutions changes sharply across this thin layer, which corresponds to a second-order regular turning point of the differential mass transport equation. In the outer zone from the inner layer down to the wall, exponentially small terms must be considered to account for the diffusive leakage of the massive species. In the inner zone, the equation is solved in terms of the Whittaker function and the whole mass fraction distribution is determined by matching with the outer solutions. The distinguished limit of Brownian diffusion with a weak thermal diffusion is also analysed and shown to match the two cases mentioned above.

1. Introduction

Ludwig, in 1856, was pioneering in discussing the phenomenon of mass thermal diffusion in liquid mixtures. Later on, and contemporary with the experiments conducted by Soret in liquid solutions subjected to a temperature gradient, the same phenomenon was first observed in gases by Tyndall (1870) and then by Aitken (1884) who reported the appearance of a dark zone surrounding lightened hot particles immersed in a dusty gas (for these early references see the monographs by de Groot 1945; or de Groot & Mazur 1984). The formation of this so called *dust-free layer* was duly related to the radiometer forces on aerosols (Rosenblatt & La Mer 1946), namely to the thermophoresis, which some time later was recognized as the particle limit of the thermal diffusion predicted in gaseous mixtures by the Enskog–Chapman solution to the Boltzmann kinetic equation (Mason & Chapman 1962). In this paper the

discussion will be centred on the dynamical behaviour of a dilute species, whose size lies on the imprecise border which separates small particles and large molecules. Thus, the terms thermophoresis, thermal diffusion and Ludwig–Soret transport will be used interchangeably to denote the *cross-transport of mass induced by a thermal gradient* and Brownian or Fickian diffusion will accordingly denote the direct diffusive mass transport due to the concentration gradients.

The importance of mass transport by thermal (Ludwig–Soret) diffusion in a variety of processes of physical and technological interest is well recognized today. The leading role played by this transport in the onset of some convective and interfacial instabilities has been exhaustively studied in fluid mixture layers subjected to a vertical temperature gradient (see for instance García-Ybarra & Velarde 1979, 1987; Castillo & Velarde 1982). The alteration of advective mass transport rates induced by thermal diffusion in non-isothermal flows has attracted special attention due to the implications for chemical vapour deposition, vapour condensation, combustion, aerosols capture/rejection by cold/hot plates, etc. (Rosner 1980, 1990; Rosner *et al*. 1992). In the combustion field, where strong and simultaneous gradients of mass and heat coexist, Ludwig–Soret transport can rarely be neglected. In fact, this has proven to be a first-order effect in a large number of phenomena related to flames (García-Ybarra 1991): in premixed flame instability (García-Ybarra, Nicoli & Clavin 1984), species concentration distribution (Fristrom & Monchick 1988), ignition by hot boundaries (García-Ybarra & Castillo 1991*a*, *b*; García-Ybarra & Treviño 1994), combustion-generated particle distribution (Castillo & García-Ybarra 1991; Rosner, Mackowski & García-Ybarra 1991; Gomez & Rosner 1993), etc. In vapour deposition problems, the influence of Ludwig–Soret transport in boundary layers has been considered by Castillo & Rosner (1988, 1989*a*, *b*), and in the crystal growth of high-molecular-weight compounds from a vapour phase by Castillo, García-Ybarra & Rosner (1992). Finally, with regard to experimental techniques and practical applications, as early as 1884 Aitken had built an air filter based on the thermophoretic capture of particles and proposed to use this phenomenon for particle removal from polluted environments. Since then, different thermophoretic precipitators have been designed (see, for instance, the recent design by Tsai & Lu 1995) which show great efficiency in collecting particles in the submicron range. In fact, some years ago, Eisner & Rosner (1985, 1986) showed that the temporal evolution of a thermocouple response induced by the thermophoretic capture of soot particles on the thermocouple bead could be used to measure the soot volume fraction in a soot-laden gas stream. Along the same lines, the thermophoretic sampling of soot particles reported by Dobbins & Megaridis (1987) is a technique widely used today (Ito, Fujita & Ito 1994). Also, in LDV measurements carried out in hot gas streams the particle and gas velocities may be substantially different due to the particle thermophoretical drift; this problem was clearly revealed by Talbot *et al*. (1980) and has been recently stressed by Sung, Law & Axelbaum (1994) in flame-related measurements.

Besides the problem of thermophoretical deposition in ducts (Walker, Homsy & Geyling 1979; Stratmann, Otto & Fissan 1994), the self-similar boundary layer with simultaneous heat and mass transfer constitutes a model problem of considerable interest in many of the practical situations mentioned above, where external flows over bluff bodies occur. Following the paper by Goren (1977) many works have been devoted to the theoretical study of the aerosol particle concentration profile in thermal boundary layers, although only partial results are known to date. Thermophoretically enhanced deposition of particles on cold surfaces was considered by Batchelor & Shen (1985) and Gökoglu & Rosner (1986*a*) among others, whereas thermophoretic

suppression of particle deposition on hot surfaces has been experimentally studied by Talbot *et al*. (1980) and theoretically by Gökoglu & Rosner (1986*b*), Park & Rosner (1989), Stratmann *et al*. (1988) and Friedlander, Fernández de la Mora & Gökoglu (1988).

When thermal diffusion is the prevailing mass transport mechanism (with Brownian diffusion playing a minor role), as in the case of a heavy species diluted in a light carrier gas, mass diffusive fluxes induced by thermal gradients appear as soon as temperature differences are appreciable in the gas mixture. Then, the concentration boundary layer thickness becomes equal to the thermal boundary layer thickness and the influence of Brownian diffusion is restricted to a thinner sublayer. In the following analysis, we show that this Brownian sublayer may be located either adjacent to the immersed body or well inside the thermal boundary layer (i.e. detached from the solid surface), depending on the thermal gradient and flow field. The aim of the present work is to provide a rather complete description of the self-similar boundary layer structure and mass transfer rates in the asymptotic limit of high Schmidt numbers. This will appear as a singular limit, which requires different expansions for the mass fraction distribution in the two kinds of differentiated regions in which the whole thermal boundary layer can be decomposed; that is, in the regions where Brownian diffusion plays a minor role (thermophoretically dominated zones) and in the Brownian sublayer. Thus, the inverse of the Schmidt number (Sc^{-1}) will be taken as the perturbation parameter to perform asymptotic expansions valid in the thermophoretic outer zones. Those will be matched with the appropriate expansions in the Brownian inner zone.

The paper is organized as follows. In §2 the contribution of thermal diffusion to the complete diffusive mass flux in a binary gas mixture is discussed. In §3 the governing equations for self-similar boundary layers leading to Falkner–Skan-type solutions are presented, and the asymptotic expansions are outlined. Sections 4 and 5 are devoted to the solution of the cases of mass transfer towards a cold and a hot wall respectively. Section 6 analyses the limit of Brownian diffusion in the presence of small temperature differences, showing the influence of a small thermophoretic transport on the structure of the boundary layer. Section 7 contains a discussion of the above results and general conclusions. Finally, the Appendix addresses the determination of the thermal diffusion factor in diluted binary mixtures with the results used in the numerical evaluations presented in §2.

2. The diffusive mass flux

In a fluid binary mixture consisting of a *carrier* component and a dilute species, the diffusive mass flux of the dilute species, $\boldsymbol{j}_m$, in the absence of strong pressure gradients, is given by (de Groot & Mazur 1984; Landau & Lifshitz 1987)

$$\boldsymbol{j}_m = -\rho D \boldsymbol{\nabla}\omega - \rho\alpha_T D\omega \boldsymbol{\nabla} \ln T, \tag{2.1}$$

where ρ is the fluid density, ω is the dilute-species mass fraction, T is the local absolute temperature, D is the binary diffusion coefficient and α_T is the thermal diffusion factor. The first term on the right-hand side of (2.1) stands for the direct Fickian diffusion flux and the second term stands for the thermal diffusion (Ludwig–Soret) cross-effect. Note that a second-order term in ω has been neglected in (2.1) because of the dilution assumption (a discussion of the 'non-diluteness' effects is available in Rosner & Park 1988). Owing to this dilution we can also neglect (in the corresponding heat diffusion flux) the reciprocal cross-transport of heat due to the concentration gradient (Dufour

effect) with respect to the direct Fourier transport because it is a first-order correction in ω. However, in (2.1) the leading contribution of the cross-mass-transport induced by a thermal gradient must be retained because its relative magnitude with respect to the Fickian transport is given by the thermal diffusion factor α_T. Although in liquid mixtures Ludwig–Soret transport often represents a rather small effect the coefficient α_T may take very large values in gas mixtures when there exists a strong disparity between the molecular masses of both species. When the dilute species is the massive component (as in the case of very heavy molecules or small particles in a gas) the Schmidt number, $Sc \equiv \nu/D$ ($\equiv$ momentum diffusivity over mass diffusivity) also takes very large values owing to the low diffusion coefficient. However, the dimensionless group $\alpha \equiv \alpha_T/Sc$ can remain positive and of order unity. Under these circumstances, Ludwig–Soret transport overwhelms Fickian diffusion and induces a mass flux down the temperature gradient; that is, toward the cooler regions.

When the diluted species are just single molecules, the value of the thermal diffusion factor α_T can be predicted via the gas kinetic theory. Furthermore, as is shown in the Appendix, these predictions match asymptotically (in the limit of very massive dilute molecules) with the results expected for small particles suspended in a gas (in the limit of very large particle Knudsen numbers).

Values of the thermal diffusion strength α obtained from the gas kinetic theory, equation (A 1), are depicted in figure 1 as a function of the species radii ratio, r_1/r_0 ($\equiv$ dilute species radius over carrier-gas molecular radius), for hard spheres and elastic collisions ($a = 0$, and thus $A^* = B^* = C^* = 1$). In the limit of very light dilute molecules the thermal diffusion strength diverges to minus infinity since α_T is negative and the Schmidt number vanishes. In the opposite limit of a relatively massive dilute species, both α_T and Sc take large values but their ratio α tends asymptotically to a constant value which depends on the interaction potential between the two species. The parameter a (fraction of diffusive inter-species molecular collisions) accounts for this dependence. It becomes clear from figure 1 that there exists a wide range of radii ratios where Fickian diffusion is very weak (the Schmidt number is large) and thermal diffusion prevails as the main diffusive transport mechanism when thermal gradients are present in the gas mixture.

The previous results cannot be directly applied to the case of small particles diluted in a gas. When the particle dimensions are smaller than (or of the order of) the gas-molecule mean free path, l, equation (A 6) provides an interpolation formula which has been shown to fit most of the particle size range (Talbot *et al.* 1980). A composite expression for the thermal diffusion strength α, valid for any radii ratio, may be obtained by adding (A 1) and (A 6) and subtracting the common part (the result for the dusty gas, given by (A 3)). To illustrate the behaviour predicted by this composite expression, we present some characteristic results in figure 2, where we have taken $A^* = B^* = 1$ and C^* given by (A 4), together with the assumption that the molecules of every species are hard spheres with equal densities. The solid lines correspond to $a = 1$ (purely diffuse collisions between unequal species) whereas the broken lines account for the opposite limit of purely specular collisions ($a = 0$). For the smaller particle sizes the results of the gas kinetic theory are recovered, being independent of the total pressure. On the other hand, the thermal diffusion strength decays as l/r_1 decreases for very large particles diluted in a gas. The larger the pressure (correspondingly, the smaller the carrier-gas mean free path) the smaller the particles affected by this decay. For typical atmospheric pressures ($l/r_0 \approx 10^3$) the thermal diffusion strength remains almost constant for a range of variation of particle radii of about three decades (from the nanometer to the micron, roughly speaking). Similar

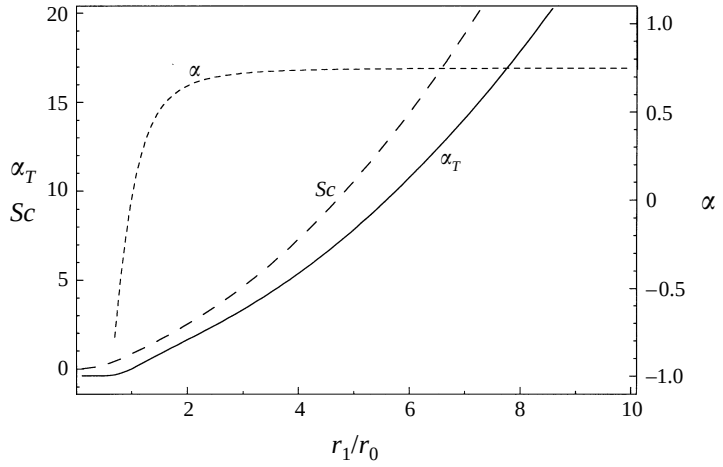

FIGURE 1. Values of the thermal diffusion factor α_T, Schmidt number Sc and thermal diffusion strength α plotted as a function of the ratio of the species radius (r_1) to carrier gas molecular radius (r_0). Results come from the gas kinetic theory for a species diluted in a carrier gas.

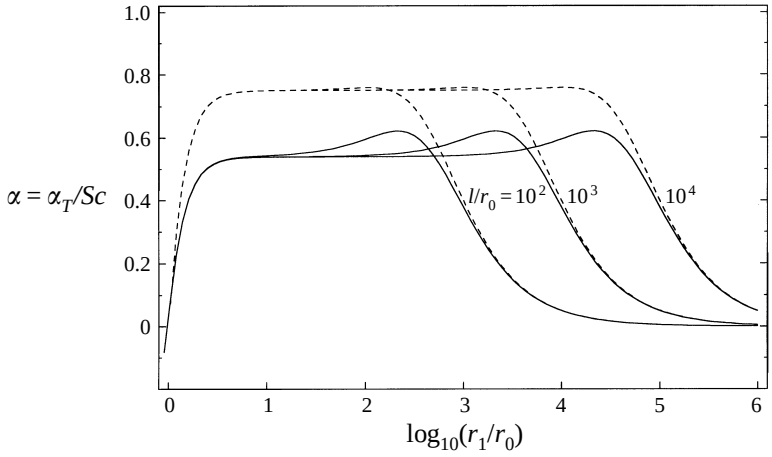

FIGURE 2. Representative values of the thermophoretic strength α for a heavy species diluted in a carrier gas plotted as a function of the ratio of the species radius (r_1) to carrier gas molecular radius (r_0). The two extreme cases of purely specular collisions ($a = 0$, dashed lines) and purely diffusive collisions ($a = 1$, solid lines) between unequal species are represented for different pressure levels measured by the ratio of mean path to molecular radius in the carrier gas.

results were discussed by Rosner & Fernández de la Mora (1982). These predictions can be compared with the experimental results collected by Talbot *et al.* (1980) in their figure 7.

Therefore, the kinetic theory formula (equation (A 1)) can be used to estimate the values of α_T and Sc in the range of sizes on which we will focus our attention in this work. That is, from large massive molecules to small particles where Fickian diffusion plays a minor role but inertia is still unimportant, i.e. the accelerations in the flow are soft enough to keep the particle Stokes number very low (for the opposite case where inertia is a dominant effect see Fernández de la Mora & Rosner 1981 and also Konstandopoulos & Rosner 1995*a*, *b*). Then, under these constraints, thermal diffusion remains as the main effect responsible for the departures of the dilute molecule (or particle) trajectories from the gas streamlines.

3. Governing equations and high-Schmidt-number asymptotics

Let us consider the two-dimensional fluid flow around a solid wedge (figure 3), where a fully developed laminar boundary layer is generated by a gas stream, with a prevailing mainstream temperature T_∞, flowing steadily on a rigid surface held at a constant temperature T_w (subscripts ∞ and w refer to values on the outer edge of the boundary layer and at the rigid wall, respectively). Let x and y denote the streamwise and normal coordinates respectively. The inviscid (potential) flow which corresponds to the neighbourhood of the forward stagnation point on a wedge with included angle equal to $\pi\beta$ (where $\beta = 2m/(m+1)$) has a streamwise velocity component of the form

$$u_\infty(x) = cx^m, \tag{3.1}$$

where c is a constant. As is well known, both the two-dimensional stagnation-region flow and the boundary layer on a flat plate at zero incidence constitute particular cases of wedge flows, the former for $\beta = 1$ (i.e. $m = 1$), the latter for $\beta = 0$ (i.e. $m = 0$). On the other hand, the case $\beta = \frac{1}{2}(m = \frac{1}{3})$ can easily be transformed into the flow near an axisymmetric stagnation point (Schlichting 1968, p. 150).

When the product of the fluid density, ρ, times the dynamic viscosity, μ, is assumed to be a constant throughout the boundary layer (that is, $\rho\mu = \rho_\infty \mu_\infty$), the similarity variable η leading to a self-similar stationary solution is obtained via the Howarth–Dorodnitysn transformation:

$$\eta = \left[\frac{(m+1)\rho_\infty u_\infty}{2\mu_\infty x}\right]^{1/2} \int_0^y (\rho/\rho_\infty)\,\mathrm{d}y. \tag{3.2}$$

The longitudinal and transverse velocity components, $\boldsymbol{v} = (u, v)$, derive from the streamfunction $\Phi(x, y)$:

$$\rho u = \rho_\infty \frac{\partial \Phi}{\partial y} \quad \text{and} \quad \rho v = -\rho_\infty \frac{\partial \Phi}{\partial x}, \tag{3.3}$$

with

$$\Phi(x, y) \equiv \left[\frac{2x\mu_\infty u_\infty}{(m+1)\rho_\infty}\right]^{1/2} f(\eta); \tag{3.4}$$

$f(\eta)$ is the dimensionless Blasius function which satisfies the differential equation

$$f''' + ff'' + \beta[\Theta - (f')^2] = 0 \tag{3.5}$$

together with the boundary conditions

$$\left.\begin{aligned} f' &\to 1 \quad \text{when} \quad \eta \to \infty, \\ f = f' &= 0 \quad \text{at} \quad \eta = 0. \end{aligned}\right\} \tag{3.6}$$

In the above relations, primes denote derivatives with respect to η. We have assumed that the gas density satisfies the equation of state for a perfect gas and have also introduced the dimensionless temperature $\Theta(\eta) \equiv T/T_\infty$, which is considered self-similar.

When the Prandtl number $Pr = \nu/\chi$ (ratio of gas kinematic viscosity, $\nu \equiv \mu/\rho$, to thermal diffusivity, χ) is taken as constant and equal to the mainstream value, the temperature profile inside the boundary layer is governed by the following differential equation:

$$\Theta'' + Pr f \Theta' = 0, \tag{3.7}$$

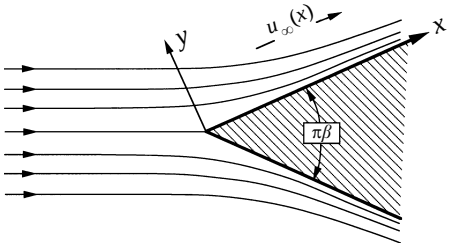

FIGURE 3. Sketch of the geometry corresponding to the two-dimensional flow of a gas around a wedge of opening angle $\pi\beta$ with a potential external flow given by $u_\infty(x) = cx^m$, with $\beta = 2m/(m+1)$.

where Θ has to satisfy the boundary conditions

$$\left.\begin{aligned} \Theta &\to 1 \quad \text{when} \quad \eta \to \infty, \\ \Theta &= \Theta_w \equiv T_w/T_\infty \quad \text{at} \quad \eta = 0. \end{aligned}\right\} \tag{3.8}$$

The solution is formally given by the Polhausen profile

$$\Theta(\eta) = \Theta_w + (1-\Theta_w)\int_0^\eta \theta(\tilde{\eta})\,\mathrm{d}\tilde{\eta} \Big/ \int_0^\infty \theta(\tilde{\eta})\,\mathrm{d}\tilde{\eta}, \tag{3.9}$$

where we have defined the function

$$\theta(\eta) \equiv \exp\left[-Pr\int_0^\eta f(\tilde{\eta})\,\mathrm{d}\tilde{\eta}\right] \tag{3.10}$$

and $\tilde{\eta}$ is a dummy integration variable.

Assuming that the mass diffusive flux is given by (2.1) and self-similarity for the normalized mass fraction distribution of the dilute species, $\Psi(\eta) \equiv \omega/\omega_\infty$, the governing boundary layer equation for Ψ becomes

$$\frac{1}{Sc}\Psi'' + f\Psi' + \alpha\frac{\mathrm{d}}{\mathrm{d}\eta}\left(\frac{\Psi}{\Theta}\Theta'\right) = 0, \tag{3.11}$$

where the Schmidt number, $Sc \equiv \nu/D$, has been assumed to be temperature independent. In (3.11), the first term corresponds to the Fickian diffusion, the second term to the advective transport and the third term comes from the thermal diffusion contribution to the mass flux.

Ψ must satisfy the boundary condition at the mainstream

$$\Psi \to 1 \quad \text{when} \quad \eta \to \infty \tag{3.12}$$

together with another boundary condition at the wall. In general, when there is a mass flux to the wall, a deposit builds up on the surface and the boundary condition accounts for the required condition on this deposit. Usually, the local mass flux to the deposit should be proportional to the departure of the mass fraction from its equilibrium value. But Ψ is assume self-similar whereas, in general, the mass flux to the wall $(-\boldsymbol{j}_m \cdot \boldsymbol{n})$ (with $\boldsymbol{n} \equiv (0,1)$ being the outward unit vector to the wall) is not self-similar and varies along the streamwise direction as $x^{(m-1)/2}$. So, only for $m = 1$ (the stagnation-point flow) is this proportionality condition compatible with a self-similar structure of the concentration boundary layer. Nevertheless, we will take a single uniform expression for the boundary condition at the wall which (while retaining the

similarity of the problem) serves to account for most of the situations encountered in practice. That is

$$J = C_S(\Psi_w - \Psi^{eq}), \tag{3.13}$$

where Ψ^{eq} stands for the value associated with the equilibrium partial pressure at the prevailing surface temperature, C_S is a kind of sticking coefficient and J is the self-similar part of the dimensionless mass flux to the wall, given by

$$J \equiv \frac{(-\boldsymbol{j}_m \cdot \boldsymbol{n})_w}{\rho_\infty \omega_\infty u_\infty}\left[\frac{2\rho_\infty u_\infty x}{(m+1)\mu_\infty}\right]^{1/2} = \frac{1}{Sc}\Psi'_w + \alpha\frac{\Psi_w}{\Theta_w}\Theta'_w. \tag{3.14}$$

Therefore, although (3.13) retains the self-similarity of the problem, only for $m = 1$ does it state the proportionality between the departure of the mass fraction from its equilibrium value and the actual local mass flux at the wall. For a different value of m, (3.13) is just a formal condition which has a physical sense only in the limits $C_S = 0$ (vanishing flux) and $C_S \to \infty$ (perfect sticking). For uniformity in the mathematical treatment of the problem we will retain (3.13) as a general boundary condition for any value of m.

When the dilute species is an aerosol forming a condensed deposit on the surface, C_S takes very large values, whereas $\Psi^{eq} \approx 0$; then, the boundary condition (3.13) corresponds to a vanishing mass fraction at the wall, $\Psi_w = 0$. On the other hand, for a dilute mixture of gases C_S becomes negligible and the boundary condition (3.13) implies that the mass flux to the wall must vanish.

Equation (3.11) can be written in the form

$$Sc^{-1}\Psi'' + G(\eta)\,\Psi' + H(\eta)\,\Psi = 0, \tag{3.15}$$

with the definitions

$$G(\eta) \equiv f + \alpha(\ln\Theta)', \tag{3.16}$$

$$H(\eta) \equiv \alpha(\ln\Theta)''. \tag{3.17}$$

In the following, equation (3.15) will be analysed by using Sc^{-1} as a smallness parameter. Thus, we will look for solutions in the form of asymptotic expansions in the limit $Sc^{-1} \to 0$, but retaining α of order unity as discussed in the previous section, in such a way that thermal diffusion and advection remain as the dominant transport mechanisms, to leading order in the Sc^{-1} expansion analysis.

Equation (3.15) is a second-order ordinary differential equation with variable coefficients. In the limit of large Schmidt number, in which we are interested, the resolution of (3.15) becomes a singular perturbation problem and the second derivative term can be neglected, at the leading algebraic order, everywhere within the viscous boundary layer except in thin diffusive sublayers where it may become relevant. Moreover, the solutions of (3.15) exhibit a different qualitative behaviour depending on the coefficient of the first derivative term, $G(\eta)$. Note that $-f(\eta)$ is the dimensionless gas velocity component along the direction normal to η. Thus, $-G(\eta)$ is equal to the addition of the normal components of the advective and the thermophoretic velocities of the dilute species. As can be seen from (3.16), the two contributions to $G(\eta)$ have a well-defined sign that remains constant throughout the boundary layer. The Blasius function, $f(\eta)$, is positive and tends to zero at the wall, whereas the thermal diffusion contribution, $\alpha(\ln\Theta)'$, can be either positive or negative leading to two different cases. In the former case, $\alpha(\ln\Theta)' > 0$ (namely, a hot stream flowing on a cold surface), the thermal diffusion flux is directed toward the surface. Adjacent to the rigid wall, a Brownian sublayer appears where the mass fraction accommodates to the value

required by the mass boundary condition (3.13). In the latter case, when advection and thermal diffusion compete, that is for $\alpha(\ln\Theta)' < 0$ (a cold stream on a hotter surface), the thermal diffusion flux is directed away from the rigid body. At some point within the boundary layer (which we will denote by η_c), the component of the advective transport normal to η is exactly balanced by thermal diffusion, and there, the function $G(\eta)$ vanishes. Then, Fickian diffusion, the second-derivative term in (3.15), should be retained in the vicinity of this point where a thin inner sublayer develops. The character of the solution changes sharply across this point, which in fact corresponds to a second-order turning point of the differential equation (3.15). Messaoudene & T'ien (1993) performed a 'patching' between the solutions in the different regions but assuming a vanishing value for the mass fraction in the zone between the internal sublayer and the wall. However, as it will be seen, in this lower region, exponentially small terms have to be considered to account for the diffusive leakage of the dilute species through the inner sublayer, as the incorporation of these small terms is crucial in the structure of the whole mass boundary layer.

In the limit $Sc^{-1} \to 0$, solutions of (3.15) can be sought in the form

$$\Psi \approx \quad (\eta)\exp[Sc\,\phi(\eta)], \tag{3.18}$$

where the function admits an expansion of the form $= {}_0 + {}_1/Sc + {}_2/Sc^2 + O(Sc^{-3})$. Substitution of (3.18) in (3.15) leads to a rather general form of the complete solution (Horn 1899) as the addition of two asymptotic series. To leading order in each series, the solution can be written as (see for instance Nayfeh 1973, p. 317 ff., and also Wasow 1965, p. 147)

$$\Psi = C_1 \exp\left(-\int_{\eta_0}^{\eta} \frac{H(\tilde\eta)}{G(\tilde\eta)}\,\mathrm{d}\tilde\eta\right) + C_2\, G(\eta)^{-1} \exp\left(\int_{\eta_0}^{\eta} \frac{H(\tilde\eta)}{G(\tilde\eta)}\,\mathrm{d}\tilde\eta\right) \exp\left(-Sc\int_{\eta_0}^{\eta} G(\tilde\eta)\,\mathrm{d}\tilde\eta\right). \tag{3.19}$$

The first term corresponds to the Sc-algebraic series resulting for $\phi'(\eta) = 0$, whereas the second term accounts for the Sc-exponential series coming from $\phi'(\eta) = -G(\eta)$, which are the two independent leading-order solutions of (3.15) in the prescribed form (3.18). The boundary conditions fix the values of constants C_1 and C_2.

The next Section is devoted to the case $\alpha(\ln\Theta)' > 0$, whereas the study of the case $\alpha(\ln\Theta)' < 0$ will be described in §5.

4. Boundary layers with thermal diffusion transport toward the wall

When the thermal diffusion transport is directed toward the wall (that is when the term $[\alpha(\ln\Theta)']$ is positive) the function $G(\eta)$ multiplying Ψ' in (3.15) is always positive and never vanishes. By choosing $\eta_0 = 0$ in (3.19), the mainstream condition, $\Psi(\infty) \to 1$, leads to

$$C_1 = \exp\left[\int_0^{\infty} \frac{H(\eta)}{G(\eta)}\,\mathrm{d}\eta\right] \tag{4.1}$$

because the Sc-exponential contribution vanishes for large values of η. However, close to the wall, this contribution becomes relevant and the boundary condition at the wall, (3.13), imposes the value of C_2:

$$C_2 = G_w\left\{\Psi^{eq} + \left(\frac{G_w}{C_S} - 1\right)\exp\left[\int_0^{\infty} \frac{H(\eta)}{G(\eta)}\,\mathrm{d}\eta\right]\right\}, \tag{4.2}$$

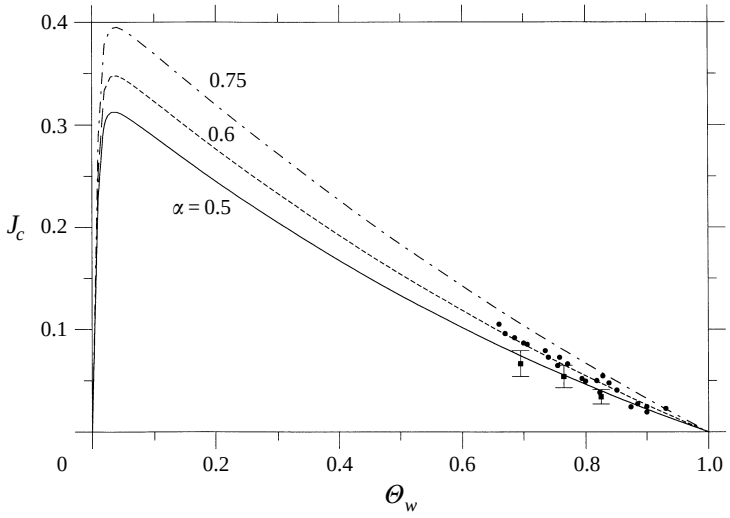

FIGURE 4. Deposition rate J_c onto a relatively cold plate (from (4.6) for $m = 0$ and $Pr = 0.7$) as a function of wall to mainstream temperature ratio (Θ_w) for three different values of the thermophoretic strength α. The dots represent the experimental data of Rosner & Kim (1984) (normalized to fit the deposition rate for $\Theta_w = 0.7$ and $\alpha = 0.6$). The squares are the experimental measurements by Konstandopoulos & Rosner (1995*b*).

where, from (3.16), G_w is given by

$$G_w \equiv G(0) = \alpha[\ln \Theta)']_w = \frac{1-\Theta_w}{\Theta_w}\frac{\alpha}{\displaystyle\int_0^\infty \theta(\eta)\,\mathrm{d}\eta}. \tag{4.3}$$

Note that because $\Theta_w < 1$, the value of G_w ranges between zero and infinity. The definite integral in the denominator has a numerical value which depends on the fluid Prandtl number Pr and on the wedge angle β (i.e. on the value of m). In the particular case of a flat plate ($m = 0$) and air ($Pr = 0.7$) the result is

$$G_w(m = 0, Pr = 0.7) = 0.4139\alpha\frac{1-\Theta_w}{\Theta_w}. \tag{4.4}$$

All the numerical results presented in this paper will correspond to these values of m and Pr.

Then, the mass fraction on the wall is

$$\Psi_w = \Psi^{eq} + \frac{G_w}{C_S}\exp\left[\int_0^\infty \frac{H(\eta)}{G(\eta)}\mathrm{d}\eta\right] \tag{4.5}$$

and the depositing mass flux on the cold wall, obtained from (3.14), is

$$J_c = G_w \exp\left[\int_0^\infty \frac{H(\eta)}{G(\eta)}\mathrm{d}\eta\right]. \tag{4.6}$$

Numerical evaluations of the deposition flux predicted by (4.6) are depicted in figure 4 for three typical values of the thermophoretic strength parameter, $\alpha = 0.5$, 0.6, and 0.75. The experimental results obtained by Rosner & Kim (1984) are indicated by filled dots (in their experimental conditions, $l/r_0 \approx 10^3$, $r_1/r_0 \approx 3 \times 10^3$, and the value $\alpha \approx 0.6$ can be estimated from our figure 2). Rosner & Kim (1984) presented their results in

relative units, by normalizing respect to the deposition rate for $\Theta_w = 0.7$. Thus, to plot their experimental results in figure 4 we have multiplied them by our theoretical value for $\Theta_w = 0.7$ (with $\alpha = 0.6$). In a more recent paper, Konstandopoulos & Rosner (1995*b*) provided further experimental deposition rate measurements which are indicated by the filled squares in figure 4. Two features of this figure should be mentioned. First, the deposition flux being proportional to G_w, it is a decreasing function of the wall temperature Θ_w almost everywhere except for very low wall temperatures where the thermophoretic deposition reaches a maximum after which, for even lower temperatures, the flux is dramatically reduced. It vanishes asymptotically in the limit of very large temperature differences ($\Theta_w \to 0$) because, owing to the exponential dependence, the thermophoretic flux becomes exponentially small (see (4.6)). Anyway, this region of very low values of Θ_w is less interesting because it is not easily achievable in actual experiments where typical temperature ratios are not lower than 0.1. Secondly, in the opposite limit of small temperature differences ($\Theta_w \to 1$), the function $H(\eta)$ becomes very small and the exponential contribution to the flux takes values close to unity. So, the limiting value of (4.6) for the thermal diffusion mass flux to a slightly cold wall vanishes like G_w:

$$J_{c,\,lim} = G_w \quad \text{when} \quad \Theta_w \to 1^-. \tag{4.7}$$

These results are valid as long as thermal diffusion is dominant. However, for very small temperature differences thermal diffusion and Brownian diffusion may become comparable. Then, the previous analysis does not give an adequate solution and, for instance, the purely Brownian (non-vanishing) deposition rate is not recovered when $\Theta_w \to 1$. The analysis of the limit of small temperature differences is performed later, in §6, to provide the connection between the hot wall and the cold wall descriptions through the isothermal case.

The previous analysis assumes that all the parameters involved in the evolution equation and boundary conditions are of order unity and the results do not properly account for the case of low sticking. The expression (4.6) for the mass flux does not depend on the sticking coefficient C_S and does not vanish when a non-sticking wall condition is imposed ($C_S \to 0$), as the boundary condition (3.13) requires. Furthermore, (4.5) shows a divergence of the mass fraction at the wall in this non-sticking limit. In fact, (3.19) was written under the assumption that the leading terms of both particular solutions of (3.15) resulting from (3.18) were of the same order in the expanding parameter Sc^{-1}. Thus, this solution cannot account for a vanishing mass flux to the wall because in that case the contribution of the exponential expansion becomes increasingly large as the sticking coefficient vanishes ($C_2 \to \infty$ when $C_S \to 0$). This divergence comes from the fact that the dilute species accumulates near the wall due to the action of thermal diffusion and, as it cannot deposit on the wall, the normalized mass fraction increases until a balance with advection is established. Then, the solution cannot be reduced to just the leading order of each particular solution (3.18), and at least three terms of the exponential series should be included. This limit of vanishing values of C_S will be considered in a future work.

5. Boundary layer with thermal diffusion transport away from the wall

When the thermal diffusion flux is directed away from the rigid surface, the contribution $\alpha(\ln \Theta)'$ is negative and the coefficient of Ψ' in equation (3.15), $G(\eta)$, vanishes at a well-defined value of the similarity variable $\eta = \eta_c$. This value corresponds to a second-order regular turning point of (3.15). Under the complete absence of

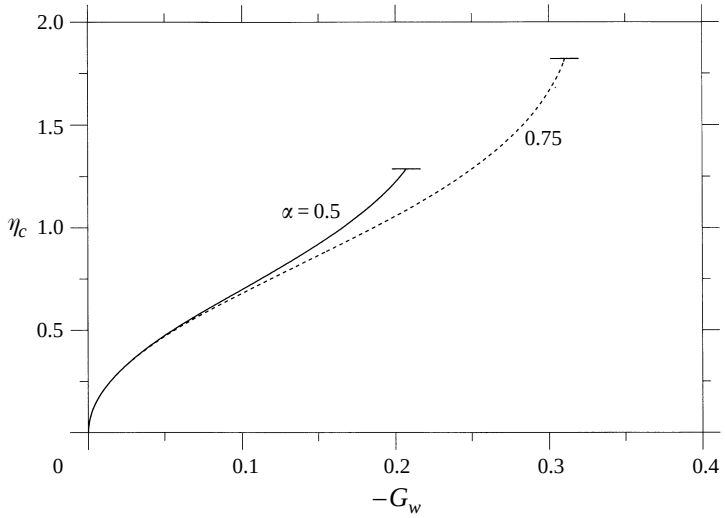

FIGURE 5. Location of the turning point η_c vs. $|G_w|$ obtained from (5.1) for $m = 0$, $Pr = 0.7$ and two values of the thermophoretic strength α. The lines end at the values of G_w corresponding to $\Theta_w \to \infty$ in (4.4).

Brownian diffusion (the case $Sc^{-1} = 0$), η_c defines the stagnation point of the dilute species, and divides the boundary layer into two distinguished zones: an upper zone above the turning point ($\eta > \eta_c$) where the dilute species is present and a lower zone (usually denoted in the literature as the *dust free layer*) between η_c and the wall where this species is absent. However, for non-vanishing (and no matter how small) Brownian diffusion, the dilute species is able to diffuse across η_c and an inner sublayer must be taken into account around η_c where diffusion becomes comparable to the combined effects of advection and thermal diffusion. The value of η_c is implicitly given by the relation

$$G(\eta_c) \equiv [f + \alpha(\ln \Theta)']_{\eta=\eta_c} = 0 \tag{5.1}$$

which is easily solved for any value of α.

For a flat-plate boundary layer, where G_w is given by (4.4), typical values of η_c versus $(-G_w)$ are shown in figure 5. The use of G_w as the independent variable is suggested by the small-temperature-gradient limit of (5.1) (see later, (5.28)). On the other hand, note that according to (4.3), the parameter G_w has a limiting value, equal to $-\alpha(\int_0^\infty \theta \, d\eta)^{-1}$, reached asymptotically in the limit of very large temperature differences ($\Theta_w \to \infty$). This extreme value depends on Pr, m and α, but is independent of the Sc value. Then, in figure 5 each curve has an end point (indicated by a horizontal bar) which corresponds to the limiting value of G_w. In fact, these limit cases provide the maximum allowed values of η_c that have been depicted in figure 6 for the corresponding values of α. They represent the maximum thickness of the dust-free layer or *dark zone* that can be achieved for a given value of α. No matter how much the rigid plate is heated, the dust-free region can only extend over a fraction of the whole thermal boundary layer.

5.1. *Outer regions*

In these zones where the turning point is excluded ($\eta \neq \eta_c$), the concentration profile is given by expressions of the type indicated by (3.19). We will use superscript $+$ to denote the solution in the upper region ($\eta > \eta_c$) and superscript $-$ for the lower region ($0 \leqslant \eta < \eta_c$). The subscript c will denote values at $\eta = \eta_c$.

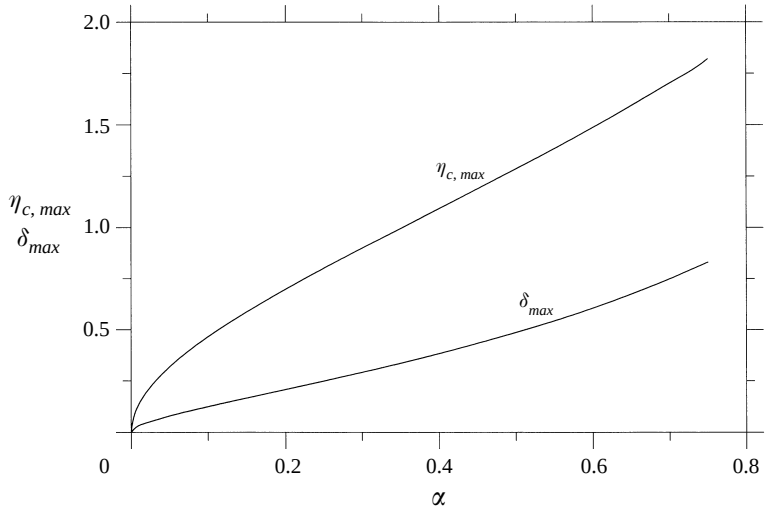

FIGURE 6. Maximum thickness of the dust free region $\eta_{c,\,max}$ and upper limit value of the parameter δ, corresponding to extremely large temperature differences ($\Theta_w \to \infty$) as a function of the thermophoretic strength α. Represented values are for $m = 0$ and $Pr = 0.7$.

In the upper region, we take $\eta_0 = \infty$ in (3.19). Then, C_2^+ must be taken equal to zero because, as $G(\eta) > 0$ in this region, this contribution diverges exponentially in Sc. On the other hand, the boundary condition at the mainstream (3.12) leads to $C_1^+ = 1$. Thus, (Goren 1977)

$$\Psi_{out}^+ = \exp\left[\int_\eta^\infty \frac{H(\tilde{\eta})}{G(\tilde{\eta})}\mathrm{d}\tilde{\eta}\right]. \tag{5.2}$$

It is interesting to note the identity

$$H(\eta) \equiv (1-\alpha\, Pr) f(\ln\Theta)' - [f+\alpha(\ln\Theta)'](\ln\Theta)'. \tag{5.3}$$

When this relation is used in (5.2) the contribution of the second term can be integrated leading to a pre-exponential factor equal to Θ, whereas the first term gives a contribution in the exponential whose sign depends on the product $\alpha\, Pr$. If this product turns out to be larger than unity (and this is a rather unusual case) the integral in (5.2) would take large and positive values when $\eta \to \eta_c$ and Ψ_{out}^+ would show a divergence close to the critical point (i.e. there would be a relative accumulation of dilute material at this position). On the other hand, when $\alpha\, Pr$ is smaller than unity, which corresponds to the physically interesting case, the integral of (5.2) takes large and negative values and the dilute-species concentration vanishes in the proximity of the locus $\eta = \eta_c$. More precisely, around η_c, and considering the Taylor expansion of $G(\eta)$,

$$G(\eta \to \eta_c) = (\eta-\eta_c)\, G_c' + O(\eta-\eta_c)^2, \tag{5.4}$$

the leading-order form of (3.15) is

$$G_c'(\eta-\eta_c)(\Psi_{out}^+)' + H_c\, \Psi_{out}^+ = 0, \tag{5.5}$$

showing that $\eta = \eta_c$ is a regular singular point of this leading-order outer equation. The solution of (5.5) is

$$\Psi_{out}^+(\eta \to \eta_c) \approx C(\eta-\eta_c)^\delta, \tag{5.6}$$

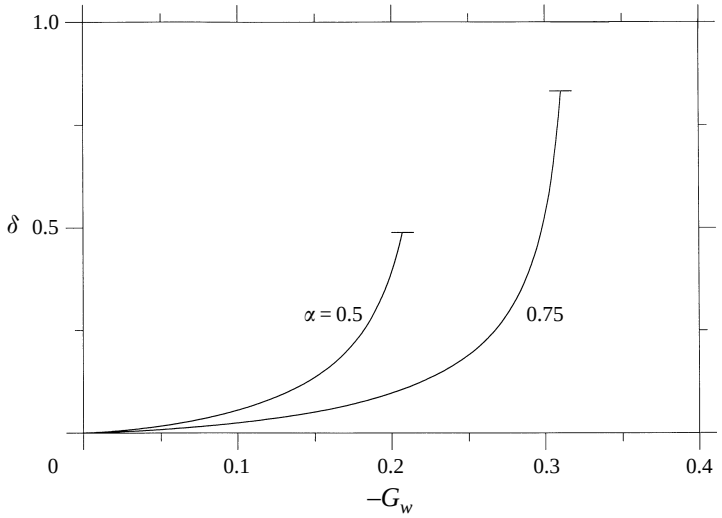

FIGURE 7. Value of the parameter δ (from (5.7), for $m = 0$ and $Pr = 0.7$) vs. $|G_w|$ for two values of the thermophoretic strength. The lines end at the values of G_w corresponding to $\Theta_w \to \infty$ in (4.4).

where C is a constant to be determined below and we have defined the parameter

$$\delta \equiv \frac{-H_c}{G_c'} \equiv \left[\frac{\alpha f_c'}{f_c^2(1-\alpha\, Pr)} - 1\right]^{-1}. \tag{5.7}$$

As can be seen from this relation, δ is positive for $\alpha\, Pr < 1$ and conversely $\delta < 0$ for $\alpha\, Pr > 1$. Typical values of this parameter for a parallel-plate boundary layer are shown in figure 7. As for η_c, the parameter δ also reaches an upper limit value (indicated by horizontal bars in figure 7) when the temperature differences become very large ($\Theta_w \to \infty$). These maximum values are plotted in figure 6 as a function of the thermal diffusion strength α, showing that the parameter δ in physical situations is always positive and smaller than unity.

Thus, let us rewrite the solution (5.2) in the equivalent form

$$\Psi_{out}^{+} = \left(\frac{\eta-\eta_c}{\eta^*-\eta_c}\right)^{\delta} \exp\left[\int_{\eta^*}^{\infty} \frac{H(\eta)}{G(\eta)}\,\mathrm{d}\eta + \int_{\eta}^{\eta^*} F(\tilde{\eta})\,\mathrm{d}\tilde{\eta}\right], \tag{5.8}$$

where η^* is any nearby point greater than η_c and we have introduced the function

$$F(\eta) \equiv \frac{H(\eta)}{G(\eta)} + \frac{\delta}{\eta-\eta_c} = \frac{\alpha(\ln\Theta)''}{f+\alpha(\ln\Theta)'} + \frac{\delta}{\eta-\eta_c}. \tag{5.9}$$

Thus the exponential term appearing in (5.8) does not contain any singularity because the function defined by (5.9) has a regular behaviour at $\eta = \eta_c$. In fact, its expansion around this point is

$$F(\eta \approx \eta_c) = \frac{H_c' + \delta G_c''/2}{G_c'} + O(\eta-\eta_c). \tag{5.10}$$

In this way, the main dependence on η has been transferred to the pre-exponential factor in the expression (5.8), which can be used to compute numerically Ψ_{out}^{+} at any value of $\eta \geqslant \eta_c$.

Therefore, the inner limit form of this outer solution is given by (5.6) with

$$C = (\eta^* - \eta_c)^{-\delta} \exp\left[\int_{\eta^*}^{\infty} \frac{H(\eta)}{G(\eta)} \,\mathrm{d}\eta + \int_{\eta_c}^{\eta^*} F(\eta)\,\mathrm{d}\eta \right]. \tag{5.11}$$

This coefficient depends on the thermophysical properties of the gas mixture and on the imposed temperature ratio, $\Theta_w = T_w/T_\infty$. Furthermore, it is independent of the value chosen for η^* by construction.

Within the lower region ($0 \leqslant \eta < \eta_c$) we take $\eta_0 = 0$ in (3.19) and using again the function $F(\eta)$ the normalized mass fraction distribution in this lower region can be written in the form

$$\Psi^-_{out} = C_1^- \left(\frac{\eta_c - \eta}{\eta_c}\right)^{\delta} \exp\left[-\int_0^{\eta} F(\tilde{\eta})\,\mathrm{d}\tilde{\eta} \right] + C_2^- \left\{ G(\eta) \left(\frac{\eta_c - \eta}{\eta_c}\right)^{\delta} \exp\left[-\int_0^{\eta} F(\tilde{\eta})\,\mathrm{d}\tilde{\eta} \right] \right\}^{-1} \exp\left[-\int_0^{\eta} Sc\, G(\tilde{\eta})\,\mathrm{d}\tilde{\eta} \right]. \tag{5.12}$$

This equation incorporates both the *Sc*-algebraic and the *Sc*-exponential leading-order contributions in the general solution, (3.19). However, as will be seen, the boundary condition (3.13) and the matching condition with the inner Brownian sublayer (5.26), will impose that both terms in (5.12) must be of the same exponentially small order. These exponentially small terms must be retained to account for the diffusive mass leakage through the inner region. The analysis by Messaoudene & T'ien (1993) overlooked these exponentially small terms and considered a vanishing mass fraction in this lower region, providing an incomplete boundary layer description which leads to the absence of the mass deposition rate on the plate.

Using (5.12) in the equation for the mass flux to the hot wall, (3.14), gives

$$J_h = C_1^- G_w. \tag{5.13}$$

According to this result, the flux to the wall is due completely to the *Sc*-algebraic contribution term in (5.12) whereas the *Sc*-exponential contribution gives no net mass flux to the wall. The boundary condition at the wall, (3.13), relates both constants C_1^- and C_2^-, leading to

$$C_1^- = \frac{\Psi^{eq} - C_2^-/G_w}{1 - G_w/C_S}. \tag{5.14}$$

The behaviour of this lower-region solution, (5.12), in the vicinity of the turning point is obtained by using the Taylor expansion of $G(\eta)$ around η_c, equation (5.4). Thus, the inner limit form of this solution is

$$\Psi^-_{out}(\eta \to \eta_c) \approx D_1(\eta_c - \eta)^{\delta} + D_2 \frac{\exp\left[-\frac{1}{2} Sc (\eta_c - \eta)^2 G'_c\right]}{(\eta_c - \eta)^{1+\delta}}, \tag{5.15}$$

where

$$\left.\begin{aligned} D_1 &= C_1^- \frac{\exp\left[-\int_0^{\eta_c} F(\eta)\,\mathrm{d}\eta \right]}{\eta_c^{\delta}}, \\ D_2 &\equiv -C_2^- \eta_c^{\delta} \frac{\exp\left\{ \int_0^{\eta_c} [F(\eta) - Sc\, G(\eta)]\,\mathrm{d}\eta \right\}}{G'_c}. \end{aligned}\right\} \tag{5.16}$$

Therefore, the mass fraction profile in the two outer regions is solved except for one constant (either D_1 or D_2) which remains free at this stage and should be determined by coupling both outer solutions through the inner one.

5.2. *Inner diffusive region*

To analyse the structure of the inner zone surrounding η_c (the Brownian sublayer) the Taylor expansions of $G(\eta)$ and $H(\eta)$, around η_c, should be introduced in (3.15). Then, it appears that the relative thickness of the inner sublayer is $O(Sc^{-1/2})$ and the appropriate stretching variable is

$$\Lambda \equiv (Sc\, G_c')^{1/2}(\eta-\eta_c). \tag{5.17}$$

By using this variable the inner form of (3.15) in the vicinity of η_c to leading order becomes

$$\frac{\mathrm{d}^2\Psi_{inn}}{\mathrm{d}\Lambda^2}+\Lambda\frac{\mathrm{d}\Psi_{inn}}{\mathrm{d}\Lambda}-\delta\Psi_{inn}=0 \tag{5.18}$$

with δ given by (5.7). Equation (5.18) can easily be transformed into the parabolic cylinder equation by taking $\mathrm{e}^{\Lambda^2/4}\Psi_{inn}(\Lambda)$ as the dependent variable. Then, the general solution can be written as the following linear combination involving the Whittaker function $U(\cdot,\cdot)$ (Abramowitz & Stegun 1972, p. 687 ff.):

$$\Psi_{inn}=\mathrm{e}^{-\Lambda^2/4}[E_1\,U(\tfrac{1}{2}+\delta,\Lambda)+E_2\,U(\tfrac{1}{2}+\delta,-\Lambda)], \tag{5.19}$$

where the constants E_1 and E_2 must be determined by matching with the outer solutions.

To perform the matching we first note the limit behaviours of solution (5.19):

$$\Psi_{inn}(\Lambda\to+\infty)\to E_1\frac{\mathrm{e}^{-\Lambda^2/2}}{\Lambda^{1+\delta}}+E_2\frac{(2\pi)^{1/2}}{\Gamma(1+\delta)}\Lambda^{\delta}, \tag{5.20}$$

$$\Psi_{inn}(\Lambda\to-\infty)\to E_1\frac{(2\pi)^{1/2}}{\Gamma(1+\delta)}(-\Lambda)^{\delta}+E_2\frac{\mathrm{e}^{-\Lambda^2/2}}{(-\Lambda)^{1+\delta}}, \tag{5.21}$$

where Γ is the usual gamma function.

5.3. *Matching conditions*

The matching between the inner-region solution and the upper outer solution is obtained by equating (5.20) and (5.6). Thus, the value of E_2 is determined as

$$E_2=\frac{\Gamma(1+\delta)}{(2\pi)^{1/2}(Sc\,G_c')^{\delta/2}}C \tag{5.22}$$

with the coefficient C given by (5.11).

On the other hand, the matching with the lower-region solution is obtained by relating (5.21) with (5.15). This matching provides the relations

$$E_1=\frac{\Gamma(1+\delta)}{(2\pi)^{1/2}(Sc\,G_c')^{\delta/2}}D_1 \tag{5.23}$$

and

$$E_2=(Sc\,G_c')^{(1+\delta)/2}D_2, \tag{5.24}$$

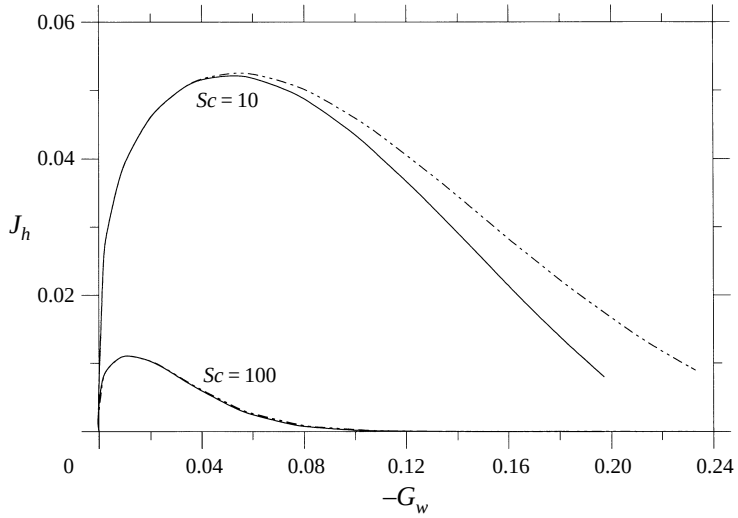

FIGURE 8. Deposition rate J_h to a hot plate (from (5.25), (5.26) for $m = 0$, $Pr = 0.7$, $\Psi^{eq} = 0$ and $C_S \to \infty$) as a function of $|G_w|$ for two different values of the Schmidt number and $\alpha = 0.5$ (solid lines) or $\alpha = 0.75$ (broken lines). For $Sc = 10^2$ both lines become indistinguishable at this scale.

with D_1 and D_2 related to C_1^- and C_2^- by (5.16). Thus, by equating (5.24) with (5.22) and using the definition (5.16) the result is

$$C_2^- = -\frac{(G_c')^{1/2-\delta}}{[(\eta^* - \eta_c)\,\eta_c]^{\delta}\, Sc^{1/2+\delta}} \frac{\Gamma(1+\delta)}{(2\pi)^{1/2}} \exp\left\{ \int_0^{\eta_c} [Sc\, G(\eta) - F(\eta)]\, \mathrm{d}\eta + \int_{\eta_c}^{\eta^*} F(\eta)\, \mathrm{d}\eta + \int_{\eta^*}^{\infty} \frac{H(\eta)}{G(\eta)}\, \mathrm{d}\eta \right\}. \quad (5.25)$$

Therefore, the constants E_2 and C_2^- are determined irrespectively of the boundary condition on the wall just by matching the two outer solutions through the inner solution.

On the other hand, the boundary condition on the wall determines the remaining constant C_1^- through its relation with C_2^- given by (5.14). Once the values of the two coefficients are known, the concentration profile in the lower outer region can be completely evaluated from (5.12) and the flux to the wall obtained from (5.13).

In the case of a depositing aerosol the flux to the hot wall is given simply by

$$J_h(\Psi^{eq} \approx 0, C_S \to \infty) = -C_2^-. \quad (5.26)$$

The computation of this particular case in a flat-plate boundary layer leads to the results depicted in figure 8, where the normalized deposition mass flux J_h is plotted versus $|G_w|$ for two Schmnidt numbers, 10 and 10^2 (which roughly correspond to large molecules and submicron particles, respectively). In each case, curves are drawn for $\alpha = 0.5$ (solid lines) and $\alpha = 0.75$ (dashed lines). For $Sc = 10^2$ both curves are indistinguishable on this scale. Thus, the relative influence of the value of α is reduced as the Schmidt number increases. This means that the uncertainties in the theoretical evaluation of α will have a minor influence on the prediction of the deposition rates to hot surfaces for sufficiently large molecules or small particles where Sc takes large values.

For very large temperature gradients, the depositing mass flux decreases exponentially to an end value corresponding to the maximum of $|G_w|$ (see (4.4)). On the

other hand, (5.26) predicts a maximum in the deposition rate for some intermediate temperature difference and even a vanishing flux in the limit of small temperature gradients ($G_w \to 0$). This result is inconsistent with the fact that even in the absence of any temperature gradient in the gas, a non-vanishing mass deposition flux produced by pure Brownian diffusion should still remain. Thus, as is the case when the thermophoretic transport is directed toward the wall (§4, equation (4.7)), the limit of small gradients of temperature cannot be simply obtained by taking the limit $G_w \to 0$ in the previous analysis and deserves a separate study that will be performed in §6. First, in the next subsection we will treat in detail the limit form reached by the species concentration distribution and mass deposition flux provided by the previous analysis for small G_w.

5.4. *The thermophoretic limit of small temperature gradients*

When the temperature difference between the wall and the gas stream is small thermal diffusion transport (which is still assumed much stronger than Brownian diffusion) becomes a weak effect and the location of η_c approaches the wall. In this case the concentration boundary layer structure described previously is notably simplified and its limit form can be analysed by taking

$$\epsilon \equiv \frac{|1-\Theta_w|}{\Theta_w} \tag{5.27}$$

as a small expansion parameter (ϵ is defined here with the absolute value in order to use the same parameter in §6). Recalling the definition of G_w, (4.3), it turns out that G_w is of order ϵ and η_c is approximately given by

$$\eta_c \approx [-2G_w/f''(0)]^{1/2}. \tag{5.28}$$

Thus, around and below η_c, the functions $G(\eta)$ and $H(\eta)$ take small values of the order of ϵ and ϵ^2, respectively. Also, the parameter δ becomes a small number of the order of $\epsilon^{3/2}$,

$$\delta \approx -G_w \eta_c \frac{1-\alpha\, Pr}{2\alpha}. \tag{5.29}$$

Note that (5.6) establishes that for small values of δ the region of the upper outer zone ($\eta > \eta_c$) where the normalized mass fraction Ψ shows an appreciable change shrinks around η_c, becoming of the same order as δ. By decreasing the value of ϵ this order may become the same as the order of the inner diffusive zone width, i.e.

$$(Sc\, G_c')^{-1/2} \approx \epsilon^{3/2}, \quad \text{that is,} \quad \epsilon = O(Sc^{-2/7}), \tag{5.30}$$

then, both zones coalesce and the leading-order solution in the outer upper zone is simply $\Psi^+_{out} = 1$. The constant C defined in (5.11) becomes equal to unity at this order.

The corresponding solution in the inner zone is obtained by taking the limit $\delta \to 0$ in the general solution (5.19), noting that in this limit the Whittaker function is related to the error function, $\mathrm{erf}(\Lambda/\sqrt{2})$.

On the other hand, the width of the lower outer zone (given by η_c) is of the order of $\epsilon^{1/2}$ and so very large compared to the inner zone thickness, $\epsilon^{3/2}$. Therefore, in this regime a well-differentiated outer zone still exists between the critical line and the wall. The limit $\epsilon \to 0$ corresponds to vanishing values of δ, $F(\eta)$ and $H(\eta)$ in (5.12). Moreover, this limit in the expression (5.13) for the mass flux to the wall with (5.14) and (5.25) leads to

$$J_{h,lim} = -G_w \frac{(\pi\Lambda)^{-1/2}\, e^{-2\Lambda/3} - \Psi^{eq}}{1 - G_w/C_S}, \tag{5.31}$$

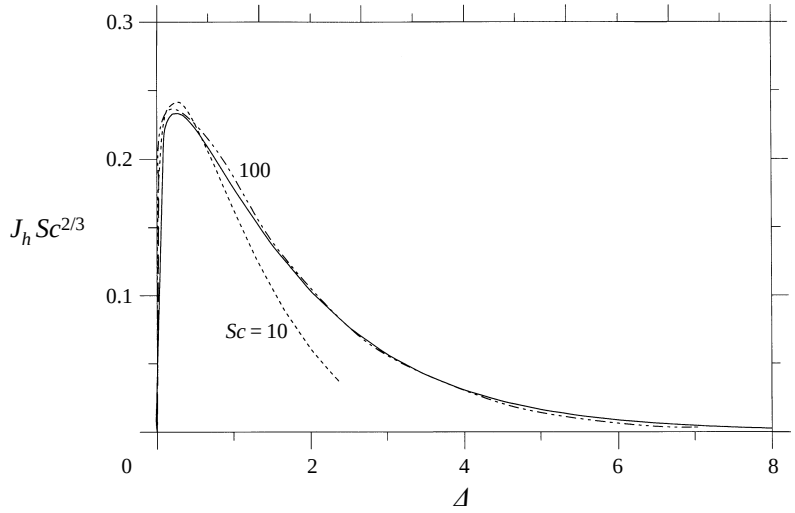

FIGURE 9. Normalized deposition rate ($J_h Sc^{2/3}$) to a hot plate (for $m = 0$, $Pr = 0.7$, $\Psi^{eq} = 0$ and $C_S \to \infty$) as a function of the parameter Δ defined by (5.32). Solid line represents $J_{h,lim}$ from (5.31) and the dashed lines accounts for J_h from (5.25), (5.26) for $Sc = 10$ and $Sc = 10^2$ with $\alpha = 0.5$.

where we have introduced the positive parameter Δ defined by (Friedlander *et al.* 1988)

$$\Delta \equiv Sc\,|G_w|\,\eta_c \tag{5.32}$$

which, in this regime, is a large parameter of order ϵ^{-2}. Thus, (5.31) shows how small the mass flux becomes in this regime of relatively small gradients of temperature. Note also that only when C_S becomes of order ϵ, does the partial impermeability of the wall start to be manifested by decreasing the mass flux.

The depositing mass flux ($J_{h,lim}$) predicted by (5.31) for an aerosol ($\Psi^{eq} \approx 0$, $C_S \to \infty$) in a parallel-plate boundary layer is shown by the solid line in figure 9. The corresponding results given by the general expression for J_h, (5.26), with $\alpha = 0.5$ are also plotted here (broken lines) in terms of the parameter Δ for two different Schmidt numbers. The comparison shows that $J_{h,lim}$ gives a very accurate prediction when Sc is around 10^2 or larger. However, for smaller values of the Schmidt number ($Sc \approx 10$) the limit expression (5.31) overpredicts the deposition flux and $J_{h,lim} > J_h$.

The validity of the previous results is restricted to large values of Δ (of order ϵ^{-2}). Then, the region near $\Delta = 0$ in figure 9 is not correctly described, and a different analysis accounting for a Brownian diffusion of the same order as (or even larger than) thermophoresis is required in this range of very small temperature gradients. The study of this case is carried out in the next Section.

6. Large-Schmidt-number limit of Brownian deposition modified by a small thermophoresis

In the limit of vanishing temperature differences between the plate and the oncoming gas the thermophoretic mass transport has to become negligible. Therefore, the purely Brownian deposition case should be recovered as the limit of no thermophoresis is approached. However, for cold (respectively hot) walls, the limit of the deposition flux provided by J_c in (4.7) (respectively J_h in (5.31)) just tends to zero when Θ_w tends to one, without accounting for any Brownian flux. The particular case of small temperature differences can be solved by taking this limit directly in the governing equation (3.15)

instead of following the general procedure indicated at the end of §3 (see (3.18)). The analysis will be valid for thermophoretic transport directed towards the wall ($G_w > 0$) as well as for thermophoretic transport directed away from the wall ($G_w < 0$) in the limit $|G_w| \ll 1$.

We can use again the parameter ϵ defined in (5.27) as a small expansion parameter. It is easy to see that the function $H(\eta)$ takes values always smaller than the function $G(\eta)$. Therefore $H(\eta)$ can be neglected in (3.15) to leading order in ϵ and then the solution of (3.15) can be written in terms of a quadrature for any value of the Schmidt number. However, in the case of small temperature differences, but still large Schmidt numbers, the influence of both thermophoresis and Brownian diffusion becomes restricted to a very thin region around the plate. The three remaining terms in (3.15) at leading order are the advective and the thermophoretic contributions to $G(\eta)$ evaluated near the wall, and the Brownian diffusion term (Ψ''/Sc). The condition that these three terms are of the same order imposes a relative ordering between ϵ and Sc:

$$\epsilon = O(Sc^{-2/3}) \tag{6.1}$$

leading to the rescaled similarity variable

$$\xi \equiv \left(\frac{f''(0)}{2|G_w|}\right)^{1/2} \eta. \tag{6.2}$$

With this rescaling, (3.15) to leading order becomes

$$\frac{\mathrm{d}^2\Psi}{\mathrm{d}\xi^2} + \Lambda(\xi^2 \pm 1)\frac{\mathrm{d}\Psi}{\mathrm{d}\xi} = 0. \tag{6.3}$$

The positive sign corresponds to $G_w > 0$ (for a relatively cold wall) and the negative sign accounts for the case $G_w < 0$ (a slightly hotter wall). The latter case was analysed by Friedlander *et al.* (1988) with the condition of vanishing mass fraction at the wall. Here, we will extend their results to more general boundary conditions and also include the case when $G_w > 0$.

In (6.3) we have used the parameter

$$\Lambda \equiv \left(\frac{2}{f''(0)}\right)^{1/2} Sc|G_w|^{3/2}. \tag{6.4}$$

For negative values of G_w this definition of Λ agrees with the previous definition (5.32), although in the actual scaling (see (6.1)) Λ is a parameter of order unity. It is worthwhile noticing that for negative values of G_w (6.3) is in fact the limit of the inner-region equation (5.18) for very small temperature differences. Equation (6.3) is now written in terms of the variable ξ, which is related to the inner variable Λ by

$$\Lambda = (2\Lambda)^{1/2}(\xi - 1). \tag{6.5}$$

In the new variable ξ the origin is shifted to the wall and the turning point is located at $\xi_c = 1$. In fact, what happens in this limit of small and negative values of G_w is that the lower outer region is embedded in the inner diffusive region because their respective thicknesses become of the same order $\epsilon^{1/2}$. Then, only two distinguished regions remain: the upper outer zone covering most of the boundary layer, where the mass fraction is constant and equal to the mainstream value, and the thin inner diffusive region (now located just on the wall), where the mass fraction changes from the mainstream value to the value required by the boundary condition on the wall. In this

limit δ is negligible and in the Taylor expansion of the function $G(\eta)$ around η_c the two first terms are of the same order and should be retained, leading to

$$G(\eta \to \eta_c) = G'_c(\eta - \eta_c) + \tfrac{1}{2}G''_c(\eta - \eta_c)^2 + o(\epsilon) \tag{6.6}$$

as G'_c is of order $\epsilon^{1/2}$ and G''_c is of order unity. Under these circumstances the physical characteristics of both cases $G_w > 0$ and $G_w < 0$ as well as the corresponding equations and boundary conditions become analogous: only two differentiated regions exist and the outer region is the same in both cases. Then a unified mathematical analysis can be performed, the only difference being the plus or minus sign in (6.3) governing the mass distribution in the inner (near-wall) region.

In general the solution of (6.3) which satisfies the mainstream condition (3.12) is

$$\Psi(\xi) = \Psi(0) + [1 - \Psi(0)]\frac{I_{\pm}(\Delta, \xi)}{I_{\pm}(\Delta, \infty)}, \tag{6.7}$$

where we have introduced the integral function

$$I_{\pm}(\Delta, \xi) \equiv \int_0^{\xi} \exp\left[-\Delta(\tfrac{1}{3}\tilde{\xi}^3 \pm \tilde{\xi})\right] \mathrm{d}\tilde{\xi}. \tag{6.8}$$

Here, the subscript $+$ stands for the case $G_w > 0$ and the subscript $-$ stands for the opposite case when $G_w < 0$. The boundary condition at the plate, (3.13), fixes the value of $\Psi(0)$, resulting in

$$\Psi(0) = \frac{\Psi^{eq} + |G_w|/C_S\, \Delta I_{\pm}(\Delta, \infty)}{1 - (|G_w|/C_S)[\pm 1 - 1/\Delta I_{\pm}(\Delta, \infty)]}. \tag{6.9}$$

Although $|G_w|$ is here a small parameter of order ϵ (i.e. of order $Sc^{-2/3}$) its contribution has been retained to account for the limit case of low sticking $C_S = O(\epsilon)$ when this contribution becomes of order unity.

In the case of large Schmidt number with Brownian diffusion modified by a small thermophoretic contribution, the deposition mass flux to the wall J_{BT} from (3.14) is

$$J_{BT} = |G_w|\frac{[1/\Delta I_{\pm}(\Delta, \infty)] + \Psi^{eq}[\pm 1 - 1/\Delta I_{\pm}(\Delta, \infty)]}{1 - (|G_w|/C_S)[\pm 1 - 1/\Delta I_{\pm}(\Delta, \infty)]}. \tag{6.10}$$

For perfect sticking ($C_S \to \infty$) and $\Psi^{eq} = 0$, (6.9) leads to a vanishing mass fraction on the wall, $\Psi(0) = 0$. Whenever $G_w < 0$ the solution (6.7) and the mass flux given by (6.10) specialize to the results found by Friedlander *et al.* (1988).

We study now the different limits of (6.10) in the cases $\Delta \to 0$ (Brownian-dominated regime) and $\Delta \to \infty$ (thermophoretically dominated regime). For vanishing values of Δ (that is, when Θ_w is close to unity) the following common limit behaviour is easily obtained from (6.8):

$$\Delta I_{\pm}(\Delta, \infty) \approx 3^{1/3}\Gamma(4/3)\,\Delta^{2/3}, \tag{6.11}$$

which is valid for positive as well as for negative G_w values. When this result is used in (6.10) the limiting expression for Brownian deposition flux in the absence of thermophoresis (J_B) is obtained:

$$J_B = Sc^{-2/3}\frac{1 - \Psi^{eq}}{[6/f''(0)]^{1/3}\,\Gamma(\frac{4}{3}) + 1/(C_S\, Sc^{2/3})}, \tag{6.12}$$

which recovers the flux in the pure Brownian regime for large Schmidt numbers.

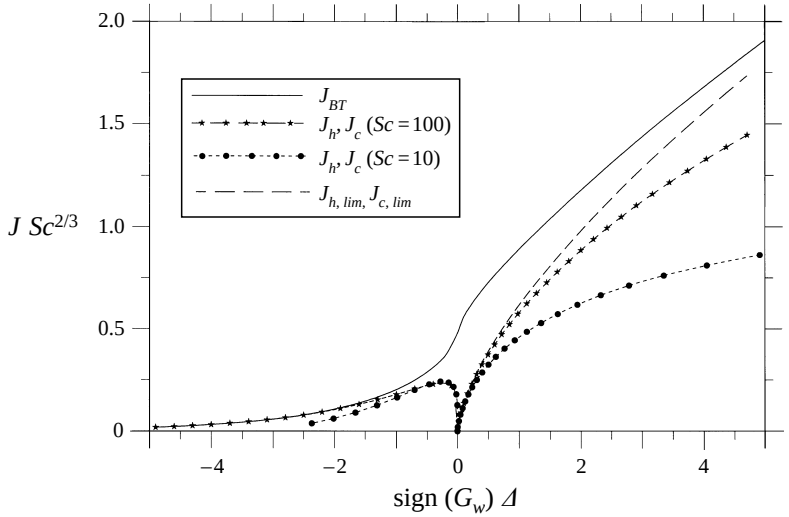

FIGURE 10. Normalized deposition rate ($J\,Sc^{2/3}$) onto a flat plate (for $m = 0$, $Pr = 0.7$, $\Psi^{eq} = 0$, $C_S \to \infty$ and $\alpha = 0.5$) as a function of the parameter Δ defined by (6.4). Positive (respectively negative) values of G_w correspond to a cold (respectively hot) plate.

For large values of the parameter Δ, the asymptotic behaviour of $I_{\pm}$ leads to (see, for instance, Bleistein & Handelsman 1986, pp. 81 and 181)

$$\Delta I_{+}(\Delta, \infty) \approx 1 - 2/\Delta^2 \quad \text{when} \quad \Delta \gg 1, \tag{6.13}$$

$$\Delta I_{-}(\Delta, \infty) \approx (\pi\Delta)^{1/2}\, e^{2\Delta/3} \quad \text{when} \quad \Delta \gg 1. \tag{6.14}$$

Therefore, the mass deposition rate given by (6.10) recovers both limits: the deposition rate on a cold surface $J_{c,lim}$ provided by (4.7) and the deposition rate on a hot wall $J_{h,lim}$ given by (5.31). These results show that there exists a perfect matching between the regime of Brownian-diffusion-dominated deposition, (6.10), and the thermophoretically dominated regimes studied in §§4 and 5.

The prediction of this Brownian case with a small temperature gradient J_{BT}, (6.10), is depicted by the solid line in figure 10 for a depositing aerosol ($\Psi^{eq} = 0, C_S \to \infty$). In this regime the deposition rate shows a strong dependence on the prevailing thermal gradients. For large Schmidt numbers, a value of Δ of order unity can be achieved with very small temperature differences (as can be seen from (6.4)). Then, the influence of thermophoresis leads to substantially different deposition rates from the purely Brownian flux. The results of figures 4 and 9 are also plotted again for comparison here in terms of the rescaled flux and temperature gradient. These latter results correspond to J_c from (4.6) and J_h from (5.26), respectively, by assuming order-unity values of G_w and are represented for $\alpha = 0.5$ in figure 10: the dashed line with the stars is for the case in which $Sc = 10^2$ and the dashed line with the solid circles corresponds to $Sc = 10$. The asymptotic limits for small absolute values of G_w($J_{c,lim}$ from (4.7) and $J_{h,lim}$ from (5.31)) are also depicted by the dashed lines in figure 10 although, in the case of $G_w < 0$, $J_{h,lim}$ is indistinguishable from J_h for $Sc = 10^2$. It is noteworthy that for large values of Δ the solid line merges with these two broken limit lines complying with the asymptotic behaviour $J_{c,lim}$ and $J_{h,lim}$ provided by (4.7) and (5.31), respectively. Thus, it is clear from this picture that the difference between the depositing flux predicted by both analyses becomes important when Δ is small as all the broken lines are different from the purely Brownian deposition rate (J_B) and provide a vanishing flux in

the absence of thermal gradients. On the other hand, when Δ is large the small-temperature-gradient result J_{BT} (represented by the solid line) overpredicts the depositing flux, which in this case is correctly described by J_c, (4.6), or J_h, (5.26). These results will be used in the next Section to construct a composite expression for the depositing mass flux (J) valid in the whole range of temperature gradients.

7. Discussion of results and conclusions

A general analysis of the thermophoretic mass transport across self-similar thermal boundary layers has been performed considering a small Brownian diffusion (that is, in the large-Schmidt-number limit). The study describes the behaviour of a species very diluted in a carrier gas and applies to suspended corpuscles with radii typically in the range 10^{-6}–10^{-9} m at 1 atm (from submicron particles to giant molecules or molecular aggregates). For this range of sizes, the Schmidt number Sc takes large values whereas the thermophoretic strength factor α becomes of order unity (see figures 1 and 2). Under these circumstances, the presence of large temperature differences in the gas induces a diffusive mass flux (the thermophoretic flux, directed down the temperature gradient) which overwhelms the pure Brownian diffusive transport (directed down the concentration gradient). Thus, for polluted gases containing particles or molecular aggregates and flowing non-isothermally over solid objects (i.e. hot combustion gases on heat exchanger surfaces or room-temperature gases on externally heated bodies in chemical vapour deposition processes) thermophoresis is the main diffusive mass transport within the thermal boundary layers near the walls. Nevertheless, Brownian diffusion cannot be completely neglected, being responsible for the accommodation of the concentration gradient at the rigid surfaces to satisfy the boundary conditions, and also playing a crucial role at locations where thermophoresis is counterbalanced by advection.

The case of two-dimensional and self-similar laminar boundary layers on cold or hot solid wedges (see figure 3) has been considered as a model problem. Expressions for the mass deposition rate and concentration profiles have been provided in terms of the external controlling parameters: the relative wall-to-gas temperature ($\Theta_w = T_w/T_\infty$), of the wedge angle (β), and of the parameters characterizing the thermophysical properties of the gas mixture: thermophoretic strength (α), Schmidt (Sc) and Prandtl (Pr) numbers, the normalized equilibrium mass fraction on the deposit (Ψ^{eq}) and a phenomenological sticking coefficient (C_S). Also, the relevant groupings of these parameters have been identified in the different regimes so as to simplify the theoretical description and the correlation of experimental results. Numerical computations were made for a parallel flat-plate boundary layer ($m = \beta = 0$) by setting $Pr = 0.7$ (a typical value for air), $\Psi^{eq} = 0, C_S \to \infty$ and two different representative values of α (0.5 and 0.75) and Sc (10 and 10^2), although from the formula provided deposition rates and concentration profiles can be obtained for any other value of the parameters. The main results are summarized below.

For *cold* bodies immersed in a hot gas stream (§4) thermophoresis induces a flux of the dilute species directed towards the body surface. For a non-vanishing sticking coefficient C_S this flux across the thermal boundary layer leads to a deposition rate to the surface J_c provided by (4.6). Characteristic values of the dimensionless deposition rate J_c were depicted in figure 4 and compared with the available experimental measurements.

For *hot* solid bodies in a relatively colder gas, thermophoresis pushes the suspended particles away from the body surface, giving birth to the so-called *dust-free* region

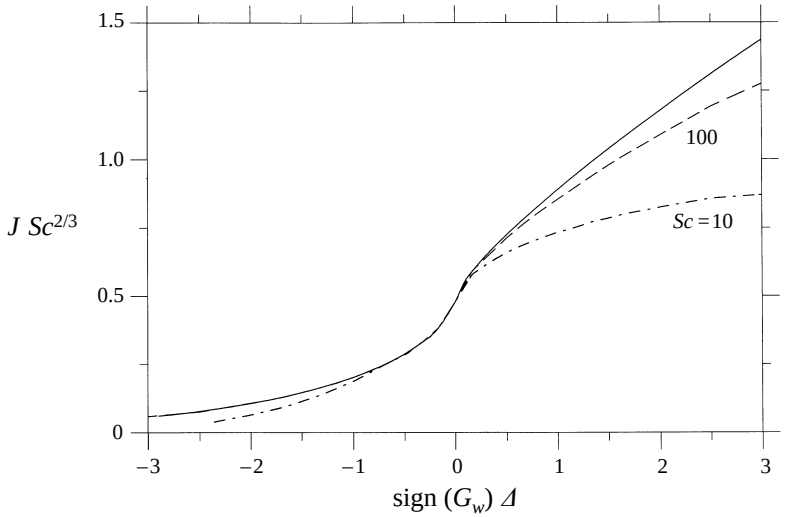

FIGURE 11. Normalized deposition rate ($J\,Sc^{2/3}$) to a flat plate (for $m = 0$, $Pr = 0.7$, $\Psi^{eq} = 0$ and $C_S \to \infty$) as a function of the parameter Δ defined by (6.4). Solid line is for J_{BT}, (6.10), and dashed lines are the composite values (7.1*a*, *b*) for $Sc = 10$ and $Sc = 10^2$ with $\alpha = 0.5$.

around the body where the dilute material is almost absent. However, Brownian diffusion produces a small leakage of the material throughout this region and induces a non-vanishing deposition rate to the solid surface (J_h). This case was analysed in §5. In the general case, the boundary layer was divided in three well-differentiated regions: an upper region, between the boundary layer outer edge and the border of the dust-free zone (whose location is implicitly given by (5.1)) where Brownian diffusion plays no role; a lower region (the dust-free zone), where exponentially small terms should be included to account for the previously mentioned diffusive leakage; and an intermediate inner region around a turning point, which connects the two previous zones. In this inner region, Brownian diffusion should be considered to leading order, because thermophoretic and advective fluxes are opposed and their components normal to the similarity variable exactly balance each other at the turning point. The proper matching between the solutions in the three regions leads to the mass fraction distribution of the dilute species within the boundary layer and to the deposition rate to the wall J_h. Characteristic numerical results for the deposition rate predicted by (5.25) and (5.26) were depicted in figure 8. The limiting behaviour for small temperature differences (but such that thermophoresis still overwhelms Brownian diffusion) $J_{h,lim}$ is given by the much more simple and analytical equation (5.31) and was represented in figure 9. The comparison between the results obtained from both formulae shows that $J_{h,lim}$ gives an accurate prediction of the deposition rate when the Schmidt number Sc is around 10^2 or larger. However, for smaller values of the Schmidt number ($Sc \approx 10$) $J_{h,lim}$ from (5.31) overpredicts the deposition flux.

In both cases (hot or cold surfaces), in the limit when the temperature differences between the wall and mainstream conditions are so small that Brownian diffusion becomes a leading-order diffusive transport mechanism, the analyses break down and incorrectly give vanishing deposition rates. The distinguished limit of very small temperature differences was studied in §6, providing the physically correct link between the hot and cold wall cases (see figure 10). The evaluation of the different limits together with the graphical representation in figure 10 suggest that the deposition rate for any ordering of the temperature difference in the Sc^{-1}-expansion may be computed

by using a composite relation which adequately combines the results obtained in the different regimes. The composite deposition rate may be obtained by adding to the general formulae the expression obtained in the Brownian limit of very small temperature gradients (J_{BT}) and subtracting their common part. That is, for cold walls

$$J = J_c + J_{BT} - J_{c,lim}, \tag{7.1a}$$

where J_c is given by (4.6), J_{BT} by (6.10), and $J_{c,lim}$ by (4.7).

On the other hand, for hot walls

$$J = J_h + J_{BT} - J_{h,lim} \tag{7.1b}$$

with J_h given by (5.25), (5.26), J_{BT} by (6.10), and $J_{h,lim}$ by (5.31).

The composite solution (7.1) is represented by the dashed lines in figure 11, for two different Schmidt numbers, $Sc = 10$ and 10^2. Also in this figure the deposition predicted by the Brownian limit of very small temperature differences J_{BT}, (6.10), is plotted by a solid line. It seems that the range of validity of J_{BT} enlarges as the Schmidt number increases. This is just an impression due to the selection of scales in the figure as Sc enters in the definition of Δ, and large values of Δ are easily obtained as Sc is larger.

Let us summarize the results in a useful recipe-like form for guiding experimental procedures for a condensing aerosol ($C_S \to \infty$, $\Psi^{\mathrm{eq}} \approx 0$). The wall temperature is related to Δ by

$$\Theta_w = \left[1 \pm \frac{\int_0^\infty \theta \, \mathrm{d}\eta}{\alpha} (\tfrac{1}{2} f''(0))^{1/3} \left(\frac{\Delta}{Sc} \right)^{2/3} \right]^{-1}, \tag{7.2}$$

where the plus (respectively minus) sign corresponds to a cold (respectively hot) plate.

For cold plates, figure 10 shows that J_c (given by (4.6)) provides good approximate values of the deposition rate to the cold surface only when Δ is sufficiently large (of the order of 10 or larger). For the parallel-plate case, with $\Delta = 10$, (7.2) leads to the values $T_w \approx 0.25 T_\infty$ and $T_w \approx 0.61 T_\infty$ for $Sc = 10$ and $Sc = 10^2$, respectively. These T_w values are estimations of the maximum wall temperatures for which (4.6) can be properly used. For even larger wall temperatures the composite relation (7.1) should be used because the Brownian contribution makes J_{BT} important. Moreover, J_{BT} becomes dominant when the temperature differences are reduced and Δ is below about 0.5. For this Δ value, (7.2) leads to $T_w \approx 0.71 T_\infty$ and $T_w \approx 0.92 T_\infty$ for $Sc = 10$ and $Sc = 10^2$, respectively. Then, when T_w takes on even larger values (closer to T_∞) J_{BT} (provided by (6.10)) is enough to accurately predict the deposition flux. For instance, in the case of a stream of hot gases at 1000 K carrying small particles with $Sc = 10^2$ or larger, (4.7) holds for wall temperatures lower than about 600 K, whereas (6.10) works for wall temperatures larger than 900 K. Between both limits (a bandwidth of 300 K) the whole composite flux expression (7.1*a*) has to be used.

In the case of deposition to hot plates (7.2) shows clearly that for each value of the Schmidt number there is a finite extreme value of Δ (when the term within the bracket vanishes), which corresponds to the limit of infinitely large wall temperatures. For the parallel-plate case and $Sc = 10$ this limit value of Δ is close to 2. Figure 10 shows that for $Sc = 10$ the composite flux expression (7.1*b*) has to be used for almost any wall temperature no matter how large it is. Only when Δ becomes lower than 0.5 (that is, for $T_w < 1.68 T_\infty$) does J_{BT} correctly predict the deposition flux, while, for $Sc = 10^2$ or larger J_{BT} can be used to get the flux for any value of Δ with great accuracy. This excellent capability of formula (6.10) to predict the mass deposition for arbitrary values

of Δ was already noted by Friedlander *et al.* (1988) when they compared this prediction with the result of a direct numerical integration of the governing equations performed by Gökoglu & Rosner (1986*a*). The reason for the wide validty of the approximation can be understood from the value of η_c represented in figure 5. Even for large temperature differences the turning point (the dark-region border) is located near the hot wall. In this near-wall region the Blasius function is well approximated by the first term in the Taylor expansion (around $\eta = 0$), which coincides with the approximation taken in the Brownian limit with low temperature differences (§6). The existence of the upper limit for the dark region border ($\eta_{c,max}$ in figure 6) is another significant result of the present analysis.

Attempts have been made to compare our theoretical predictions with the available experimental data. The deposition study of particles on cold surfaces by Rosner & Kim (1984) and the more recent results by Konstandopoulos & Rosner (1995*b*) were compared with our theoretical predictions in figure 4. Moreover, Talbot *et al.* (1980) provided some measurements of the dust-free layer thickness observed in an aluminium-oxide-particle seeded gas stream on a heated plate. They found that almost independently of the plate temperature, the locus of the particle-free layer boundary was nicely fitted by the value of the similarity variable for which $u/u_\infty = 0.5$. This location corresponds to $\eta_c \approx 1.1$ approximately. The comparison with the theoretical predictions shown in figure 5 leads to $0.83 < \eta_c < 0.92$ (for $\alpha = 0.5$) or $1.05 < \eta_c < 1.15$ (for $\alpha = 0.75$). The agreement is very good in this latter case, which means that probably the seed particles used in the experiment had a thermophoretic strength parameter close to 0.75 (i.e. the diffuse collision fraction between the carrier gas molecules and the seed particles was close to zero, $a \approx 0$). The dark zone observed in a seeded diffusion flame by Gomez & Rosner (1993) constitutes a related experiment which provides some insights not only into the thickness of the dust-free layer but also into the diffusive inner zone, which agree with the values suggested by the present analysis.

Thus, we have discussed the importance of thermal diffusion in the distribution and deposition rate of materials carried by gas streams on solid obstacles. A first extension of this study will consist in the incorporation of the slight inertial effects that should modify the behaviour of particles in the micron range, where thermophoresis still remains dominant. These inertial effects and some other extensions such as the evolution in the shape, porosity, surface roughness or thermal properties of the solid deposit induced by the material being deposited will be the subject of follow-on studies.

Work supported by the 'Dirección General de Investigación Científica y Técnica' (DGICYT, Ministry of Education and Science (Spain)) under contracts PB91-0221 and PB94-0113. The authors want to thank Professor Daniel E. Rosner for many stimulating discussions which were the embryo of this paper, and for his hospitality during several summer stays in his laboratory (High Temperature Chemical Reaction Engineering Laboratory, Yale University) where the paper originated to a large extent. NATO Collaborative Grants CRG900615 and CRG960054, which provided partial support for these stays are also acknowledged. Finally, we are very indebted to Professor J. Fernández de la Mora (Yale University) for a critical reading of the manuscript and to Professor J. C. Antoranz (UNED) whose valuable insights and comments helped us to clarify some of the results pointed out in this paper.

Appendix. Thermal diffusion factor α_T of small particles from the molecular regime to the near-continuum limit

At the leading order of the kinetic theory of gases (Ferziger & Kaper 1972, p. 225), the thermal diffusion factor α_T of a dilute trace species in a carrier gas is

$$[\alpha_T]_{KT} = (6C^*-5)\frac{\frac{3}{2}Sc(m_1/m_0)(15m_1/m_0+8A^*-15)-5(m_1/m_0+1)}{30(m_1/m_0)^2+16A^*m_1/m_0+25-12B^*}. \quad \text{(A 1)}$$

In (A 1), m_0 and m_1 are the molecular mass of the carrier gas and of the dilute species, respectively and Sc is the Schmidt number of the mixture. The coefficients A^*, B^* and C^* depend on the nature of the intermolecular potentials and are equal to unity in the special case of hard spheres undergoing elastic collisions.

Equation (A 1) leads to two different limit values in the opposite cases of light and heavy dilute species; the corresponding limiting behaviours are

$$\frac{m_1}{m_0}\to 0, \quad [\alpha_T]_{KT}\to -(6C^*-5)\frac{5}{25-12B^*}, \quad \text{(A 2)}$$

$$\frac{m_1}{m_0}\to \infty, \quad [\alpha_T]_{KT}\to (6C^*-5)\tfrac{3}{4}Sc. \quad \text{(A 3)}$$

For hard spheres and elastic collisions these expressions reduce to $-\frac{5}{13}$ and $\frac{3}{4}Sc$, respectively.

When the dilute species is the massive one the binary diffusion coefficient D becomes very small and the Schmidt number Sc diverges in that limit. Then, (A 3) establishes that the thermal diffusion factor diverges too, but in such a way that the ratio $\alpha \equiv \alpha_T/Sc$ remains of order unity. This limit of a very heavy species diluted in a light carrier gas is known as the dusty gas or quasi-Lorentzian gas model (Mason 1957; Mason & Chapman 1962). In this particular case the calculations have been carried through for hard spheres, accounting even for the inelastic collisions, by Monchick, Yun & Mason (1963). They found

$$[6C^*-5]_{DG} = (1+a\pi/8)^{-1}, \quad \text{(A 4)}$$

where a is the fraction of the carrier gas molecules that rebound diffusely from the dust particle. Subscript DG stands for this dusty gas limit. The above result agrees with Waldmann's (1961) calculations who adopted the different procedure of adding up all the impulses transferred to a dust particle by the impinging gas molecules (Epstein 1924; García-Ybarra & Rosner 1989). Note that in this limit $[\alpha_T]_{DG}$ does not really depend on a (fraction of inelastic collisions) because the Schmidt number is also affected by exactly the same factor through the diffusion coefficient (Epstein 1924; García-Ybarra & Rosner 1989), which is given by

$$[D]_{DG} = (1+a\pi/8)^{-1}[D]_{elastic}. \quad \text{(A 5)}$$

Nevertheless, the thermophoretic force proportional to the product $\alpha_T D$ is diminished by the factor $(1+a\pi/8)^{-1}$ with respect to the case without inelastic collisions.

This dusty gas model corresponds to the large-molecular-size limit of a dilute species in the kinetic theory approach (A 3) and must also coincide with the limit of small particles in a gas, in the transition region between the free molecule and the near-continuum regimes (creeping flow). Although a complete theory is not available in this

range of Knudsen numbers we can use the interpolation formulae proposed by Talbot *et al.* (1980) from the near-continuum theory,

$$\left[\frac{\alpha_T}{Sc}\right]_{NC} = 2Q_s \frac{(\lambda_g/\lambda_p + Q_t\, l/R)[1+(l/R)(A+B\,\mathrm{e}^{-QR/l})]}{(1+3Q_m\, l/R)(1+2\lambda_g/\lambda_p + 2Q_t\, l/R)}, \tag{A 6}$$

where the subscript NC refers to the near continuum limit, λ_g and λ_p are the thermal conductivities of the carrier gas and of the particle, respectively, R is the particle radius, l is the carrier-gas mean free path, and the constants Q_s, Q_t and Q_m as well as A, B and Q are coefficients which depend on the nature of the particle–gas molecule collisions. Thus, if we impose

$$\lim_{l/R\to\infty}\left[\frac{\alpha_T}{Sc}\right]_{NC} \to \left[\frac{\alpha_T}{Sc}\right]_{DG} \tag{A 7}$$

we get the relation

$$\frac{Q_s(A+B)}{3Q_m} = \frac{3}{4(1+a\pi/8)}. \tag{A 8}$$

On the other hand, if the same requirement is imposed on the diffusion coefficient,

$$\lim_{l/R\to\infty}[D]_{NC} \to [D]_{DG} \tag{A 9}$$

by using the Millikan formula (Millikan 1923) for $[D]_{NC}$ the following relation is obtained:

$$A+B = \frac{45\pi}{64(1+a\pi/8)}. \tag{A 10}$$

When (A 10) is used in (A 8), we arrive at

$$\frac{Q_s}{Q_m} = \frac{16}{5\pi}. \tag{A 11}$$

This result and that of (A 10) are in close agreement with the results from theoretical analyses ($A+B=1.58$ for $a=1, Q_s=1.17, Q_m=1.14$, see the summary in Talbot *et al.* 1980).

Then, both the kinetic theory result (A 1) and the interpolation formulae (A 6) with the constraints imposed by (A 10) and (A 11) contain the same description of the dusty gas model in the overlapping region corresponding to intermediate Knudsen numbers. The agreement allows a formal composite expression to be written which is valid in the whole range of Knudsen numbers, as

$$\alpha \equiv \frac{\alpha_T}{Sc} = \left[\frac{\alpha_T}{Sc}\right]_{KT} + \left[\frac{\alpha_T}{Sc}\right]_{NC} - \left[\frac{\alpha_T}{Sc}\right]_{DG}. \tag{A 12}$$

Unfortunately, the practical use of (A 12) is limited because the coefficients A^*, B^* and C^* appearing in $[\alpha_T/Sc]_{KT}$, (A 1), are not known when inelastic collisions are involved. Nevertheless, it can be used to get accurate estimates of the thermal diffusion strength (α) in dilute gaseous binary mixtures when the typical size of the individual constituents of the dilute component ranges from the molecular size to particles (see §2).

REFERENCES

Abramowitz, M. & Stegun, I. 1972 *Handbook of Mathematical Functions*. Dover.

Aitken, J. 1884 On the formation of small clear spaces in dusty air. *Trans. R. Soc. Edinb.* **32**, 239–272.

Batchelor, G. K. & Shen, C. 1985 Thermophoretic deposition of particles in gas flowing over cold surfaces. *J. Colloid Interface Sci.* **107**, 21–37.

Bleistein, N. & Handelsman, R. A. 1986 *Asymptotic Expansions of Integrals*. Dover.

Castillo, J. L. & García-Ybarra, P. L. 1991 Boundary layer diffusion flames with soot particle stagnation. In *Flame Structure* (ed. O. P. Korbeinichev), vol. 2, pp. 500–503. Novosibirsk: Nauka.

Castillo, J. L., García-Ybarra, P. L. & Rosner, D. E. 1992 Morphological instability of a thermophoretically growing deposit. *J. Cryst. Growth* **116**, 105–126.

Castillo, J. L. & Rosner, D. E. 1988 A nonequilibrium theory of surface deposition from particle-laden dilute condensible saturated vapor-containing laminar boundary layers. *Intl J. Multiphase Flow* **14**, 99–120.

Castillo, J. L. & Rosner, D. E. 1989*a* Equilibrium theory of surface deposition from particle-laden dilute, saturated vapor containing laminar boundary layer. *Chem. Engng Sci.* **44**, 939–956.

Castillo, J. L. & Rosner, D. E. 1989*b* Theory of surface deposition from a unary dilute vapor-containing stream allowing for condensation within the laminar boundary layer. *Chem. Engng Sci.* **44**, 925–937.

Castillo, J. L. & Velarde, M. G. 1982 Buoyancy-thermocapillary instability: the role of the interfacial deformation in one- and two-component fluid layers heated from below or above. *J. Fluid Mech.* **125**, 463–474.

Dobbins, R. A. & Megaridis, C. M. 1987 Morphology of flame-generated soot as determined by thermophoretic sampling. *Langmuir* **3**, 254–259.

Eisner, A. D. & Rosner, D. E. 1985 Experimental studies of soot particle thermophoresis in nonisothermal combustion gases using thermocouple response techniques. *Combust. Flame* **61**, 153–166.

Eisner, A. D. & Rosner, D. E. 1986 Experimental and theoretical studies of submicron particle thermophoresis in combustion gases. *PhysicoChem. Hydrodyn.* **7**, 91–100.

Epstein, P. S. 1924 On the resistance experienced by spheres in their motion through gases. *Phys. Rev.* **23**, 710–733.

Fernández de la Mora, J. & Rosner, D. E. 1981 Inertial deposition of particles revisited and extended: Eulerian approach to a traditionally Lagrangian problem. *PhysicoChem. Hydrodyn.* **2**, 1–21.

Ferziger, J. H. & Kaper, H. G. 1972 *Mathematical Theory of Transport Processes in Gases*. North Holland.

Friedlander, S. K., Fernández de la Mora, J. & Gökoglu, S. A. 1988 Diffusive leakage of small particles across the dust-free layer near a hot wall. *J. Colloid Interface Sci.* **125**, 351–355.

Fristrom, R. M. & Monchick, L. 1988 Two simple approximations to the thermal diffusion factor and their applications to flame studies. *Combust. Flame* **71**, 89–99.

García-Ybarra, P. L. 1991 The effect of cross mass (Soret) transport on the initiation, propagation and stability properties of a combustion wave. In *Nonlinear Wave Processes in Excitable Media* (ed. A. V. Holden, M. Markus & H. G. Othmer), pp. 409–421. Plenum Press.

García-Ybarra, P. L. & Castillo, J. L. 1991*a* Flat plate boundary layer ignition with fuel thermal diffusion. In *Dynamics of Deflagration and Reactive Systems: Flames* (ed. A. L. Kuhl, J.-C. Leyer, A. A. Borisov & W. A. Sirignano), pp. 71–85. AIAA.

García-Ybarra, P. L. & Castillo, J. L. 1991*b* Influence of thermal diffusion on combustible gas ignition by a hot plate. In *Flame Structure* (ed. O. P. Korbeinichev), vol. 2, pp. 354–357. Novosibirsk: Nauka.

García-Ybarra, P. L., Nicoli, C. & Clavin, P. 1984 Soret and dilution effects on premixed flames. *Combust Sci. Tech.* **42**, 87–109.

García-Ybarra, P. L. & Rosner, D. E. 1989 Thermophoretic properties of nonspherical particles and large molecules. *AIChE J.* **35**, 139–147.

García-Ybarra, P. L. & Treviño, C. 1994 Analysis of the thermal diffusion effects on the ignition of hydrogen-air mixtures in the boundary layer of a hot flat plate. *Combust. Flame* **96**, 293–303.

García-Ybarra, P. L. & Velarde, M. G. 1979 The role of Soret and Dufour effects on the stability of a binary gas layer heated from below or above. *Geophys. Astrophys. Fluid Dyn.* **13**, 83–94.

García-Ybarra, P. L. & Velarde, M. G. 1987 Oscillatory Marangoni–Bénard interfacial instability and capillary gravity waves in single- and two-component liquid layers with or without Soret thermal diffusion. *Phys. Fluids* **30**, 1649–1655.

Gökoglu, S. A. & Rosner, D. E. 1986*a* Thermophoretically augmented mass transfer rates to solid walls across laminar boundary layers. *AIAA J.* **24**, 172–179.

Gökoglu, S. A. & Rosner, D. E. 1986*b* Prediction and rational correlation of thermophoretically reduced particle mass transfer to hot surfaces across laminar or turbulent forced-convection gas boundary layers. *Chem. Engng Commun.* **44**, 107–119.

Gomez, A. & Rosner, D. E. 1993 Thermophoretic effects on particles in counterflow laminar diffusion flames. *Combust. Sci. Tech.* **89**, 335–362.

Goren, S. L. 1977 Thermophoresis of aerosol particles in the laminar boundary layer on a flat plate. *J. Colloid Interface Sci.* **61**, 77–85.

Groot, S. R. de 1945 *L'Effet Soret, Diffusion Thermique dans les Phases Condensées*. North Holland.

Groot, S. R. de & Mazur, P. 1984 *Non-Equilibrium Thermodynamics*, 2nd edn. Dover.

Horn, J. 1899 Ueber eine lineare Differentialgleichung zweiter Ordnung mit einem wiilkurlichen Parameter. *Math. Ann.* **52**, 271–292.

Ito, H., Fujita, O. & Ito, K. 1994 Agglomeration of soot particles in diffusion flames under microgravity. *Combust. Flame* **99**, 363–370.

Konstandopoulos, A. G. & Rosner, D. E. 1995*a* Inertial effects on thermophoretic transport of small particles to walls with streamwise curvature-I: Theory. *Intl J. Heat Mass Transfer* **38**, 2305–2315.

Konstandopoulos, A. G. & Rosner, D. E. 1995*b* Inertial effects on thermophoretic transport of small particles to walls with streamwise curvature-II: Experiment. *Intl J. Heat Mass Transfer* **38**, 2317–2327.

Landau, L. D. & Lifshitz, E. M. 1987 *Fluid Mechanics*, 2nd edn. Pergamon.

Mason, E. A. 1957 Higher approximations for the transport properties of binary gas mixtures II. Applications. *J. Chem. Phys.* **27**, 782–790.

Mason, E. A. & Chapman, S. 1962 Motion of small suspended particles in nonuniform gases. *J. Chem. Phys.* **36**, 627–632.

Messaoudene, N. A. & T'ien, J. S. 1993 Diffusion layer structure in a thermophoretically affected flow over a hot surface. In *Instabilities and Turbulence in Engineering Flows* (ed. D. E. Ashpis), pp. 351–365. Kluwer.

Millikan, R. A. 1923 The general law of fall of a small spherical body through a gas, and its bearning upon the nature of molecular reflection from surfaces. *Phys. Rev.* **22**, 1–23.

Monchick, L., Yun, K. S. & Mason, E. A. 1963 Formal kinetic theory of transport phenomena in polyatomic gas mixtures. *J. Chem. Phys.* **39**, 654–669.

Nayfeh, A. 1973 *Perturbation Methods*. John Wiley & Sons.

Park, H. M. & Rosner, D. E. 1989 Combined inertial and thermophoretic effects on particle deposition rates in highly loaded dusty-gas systems. *Chem. Engng Sci.* **44**, 2233–2244.

Rosenblatt, P. & La Mer, V. K. 1946 Motion of a particle in a temperature gradient; thermal repulsion as a radiometer phenomenon. *Phys. Rev.* **70**, 385–395.

Rosner, D. E. 1980 Thermal (Soret) diffusion effects on interfacial mass transport rates. *PhysicoChem. Hydrodyn.* **1**, 159–185.

Rosner, D. E. 1990 *Transport Processes in Chemically Reacting Flow Systems*. Butterworth-Heinemann.

Rosner, D. E. & Fernández de la Mora, J. 1982 Small particle transport across turbulent nonisothermal boundary layers. *Trans. ASME: J. Engng for Power* **104**, 885–894.

Rosner, D. E. & Kim, S. 1984 Optical experiments on thermophoretically augmented submicron particle deposition from 'dusty' high temperature gas flows. *Chem. Engng J.* **29**, 147–157.

ROSNER, D. E., MACKOWSKI, D. W. & GARCÍA-YBARRA, P. 1991 Size- and structure-insensitivity of the thermophoretic transport of aggregated 'soot' particles in gases. *Combust. Sci. Tech.* **80**, 87–101.

ROSNER, D. E., MACKOWSKI, D. W., TASSOPOULOS, M., CASTILLO, J. & GARCÍA-YBARRA, P. 1992 Effects of heat transfer on the dynamics and transport of small particles suspended in gases. *I & EC Res.* **31**, 760–769.

ROSNER, D. E. & PARK, H. M. 1988 Thermophoretically augmented mass-, momentum- and energy-transfer rates in high particle mass loaded laminar forced convection systems. *Chem. Engng Sci.* **43**, 2689–2704.

SCHLICHTING, H. 1968 *Boundary Layer Theory*. McGraw Hill.

STRATMANN, F., FISSAN, H., PAPPERGER, A. & FRIEDLANDER, S. 1988 Suppression of particle deposition to surfaces by the thermophoretic force. *Aerosol Sci. Tech.* **9**, 115–121.

STRATMANN, F., OTTO, E. & FISSAN, H. 1994 Thermophoretical and diffusional particle transport in cooled laminar tube flow. *J. Aerosol Sci.* **25**, 1305–1319.

SUNG, C. J., LAW, C. K. & AXELBAUM, R. L. 1994 Thermophoretic effects on seeding particles in LDV measurements of flames. *Combust. Sci. Tech.* **99**, 119–132.

TALBOT, L., CHENG, R. K., SCHEFER, R. W. & WILLIS, D. R. 1980 Thermophoresis of particles in a heated boundary layer. *J. Fluid Mech.* **101**, 737–758.

TSAI, C.-J. & LU, H.-C. 1995 Design and evaluation of a plate-to-plate thermophoretic precipitator. *Aerosol Sci. Tech.* **22**, 172–180.

TYNDALL, J. 1870 On dust and disease. *Proc. R. Inst. Gt. Br.* **6**, 1–14.

VAN DYKE, M. 1975 *Pertubation Methods in Fluid Mechanics*. The Parabolic Press.

WALDMANN, L. 1961 On the motion of spherical particles in nonhomogeneous gases. In *Rarefied Gas Dynamics* (ed. L. Talbot), pp. 323–344. Academic.

WALKER, K. L., HOMSY, G. M. & GEYLING, F. T. 1979 Thermophoretic deposition of small particles in laminar tube flow. *J. Colloid Interface Sci.* **69**, 138–147.

WASOW, W. 1965 *Asymptotic Expansions for Ordinary Differential Equations*. Interscience. (Republished by Dover in 1987.)